TAGLN2 regulates T cell activation by stabilizing the actin cytoskeleton at the immunological synapse

Bo-Ra Na,[1] Hye-Ran Kim,[1] Indre Piragyte,[1] Hyun-Mee Oh,[2] Min-Sung Kwon,[1] Uroos Akber,[1] Hyun-Su Lee,[1] Do-Sim Park,[3] Woo Keun Song,[1] Zee-Yong Park,[1] Sin-Hyeog Im,[3,4] Mun-Chual Rho,[5] Young-Min Hyun,[6] Minsoo Kim,[6] and Chang-Duk Jun[1]

[1]School of Life Sciences, Immune Synapse Research Center and Cell Dynamics Research Center, Gwangju Institute of Science and Technology (GIST), Gwangju 500-712, South Korea
[2]Bioindustrial Process Research Center, Korea Research Institute Bioscience and Biotechnology (KRIBB), Jeongeup 580-185, South Korea
[3]Academy of Immunology and Microbiology (AIM), Institute for Basic Science (IBS), Pohang 790-784, South Korea
[4]Division of Integrative Biosciences and Biotechnology (IBB), Pohang University of Science and Technology, Pohang 790-784, South Korea
[5]Department of Laboratory Medicine, School of Medicine, Wonkwang University, Iksan 570-749, South Korea
[6]Department of Microbiology and Immunology, David H. Smith Center for Vaccine Biology and Immunology, University of Rochester, Rochester, NY 14642

The formation of an immunological synapse (IS) requires tight regulation of actin dynamics by many actin polymerizing/depolymerizing proteins. However, the significance of actin stabilization at the IS remains largely unknown. In this paper, we identify a novel function of TAGLN2—an actin-binding protein predominantly expressed in T cells—in stabilizing cortical F-actin, thereby maintaining F-actin contents at the IS and acquiring LFA-1 (leukocyte function-associated antigen-1) activation after T cell receptor stimulation. TAGLN2 blocks actin depolymerization and competes with cofilin both in vitro and in vivo. Knockout of TAGLN2 (*TAGLN2*$^{-/-}$) reduced F-actin content and destabilized F-actin ring formation, resulting in decreased cell adhesion and spreading. *TAGLN2*$^{-/-}$ T cells displayed weakened cytokine production and cytotoxic effector function. These findings reveal a novel function of TAGLN2 in enhancing T cell responses by controlling actin stability at the IS.

Introduction

Activated T cells play a central role in adaptive immunity through cytokine secretion or the destruction of antigen-bearing cells. T cell activation and function require physical contact with antigen-presenting cells (APCs) at a specialized junction structure known as the immunological synapse (IS; Monks et al., 1998; Grakoui et al., 1999). Once formed, signal-dependent rearrangements in actin cytoskeleton dynamics are absolutely necessary to sustain correct temporal and spatial control of the activation process (Huang and Burkhardt, 2007; Yu et al., 2013). Alteration of actin dynamics at the IS results in immune dysfunction.

Our understanding of actin cytoskeleton reorganization during T cell activation has advanced rapidly in the last decade by adding new players and gaining mechanistic insight into T cell biology. The actin-related protein 2/3 (Arp2/3) complex is a major regulator of actin dynamics in T cells, as in other cell types (Higgs and Pollard, 2001). Of the Arp2/3-activating factors, WASp (Wiskott–Aldrich syndrome protein), WIP (WASP-interacting protein), WAVE (WASP-family verprolin-homologous protein), and HS1 (hematopoietic lineage cell-specific protein 1) are well studied in T cells, and depletion of these proteins individually results in poor actin polymerization and weakens the ability of T cells to form the IS with APCs (Huang and Burkhardt, 2007). Formins are a class of actin nucleators that are independent of Arp2/3 (Pruyne et al., 2002). Two formins, mDia1 and FMNL-1 (formin like-1), are necessary for microtubule-organizing center translocation toward the IS, whereas their depletion has no effect on the development of normal lamellipodium and IS (Gomez et al., 2007). Additionally, several negative regulators of F-actin have been described in T cells (Ichetovkin et al., 2002; Eibert et al., 2004). Cofilin is well

Correspondence to Chang-Duk Jun: cdjun@gist.ac.kr

Abbreviations used in this paper: ABM, actin-binding motif; APB, actin polymerization buffer; APC, antigen-presenting cell; Arp2/3, Actin-related protein 2/3; CFSE, carboxyfluorescein succinimidyl ester; CH, calponin homology; CMV, cytomegalovirus; Cyt D, cytochalasin D; DCs, dendritic cells; d-SMAC, distal SMAC; ERK, extracellular signal–regulated kinase; ES, embryonic stem; G-actin, globular actin; IS, immunological synapse; OVA, ovalbumin; PBLs, peripheral blood lymphocytes; PerCP, peridinin chlorophyll protein complex; PI3K, phosphoinositide 3-kinase; PLL, poly-L-lysine; qPCR, quantitative PCR; SEB, *Staphylococcal aureus* enterotoxin B; SEE, *Staphylococcal aureus* enterotoxin E; SMAC, supramolecular activation cluster; TCR, T cell receptor; WT, wild type.

The Rockefeller University Press $30.00
J. Cell Biol. Vol. 209 No. 1 143–162
www.jcb.org/cgi/doi/10.1083/jcb.201407130

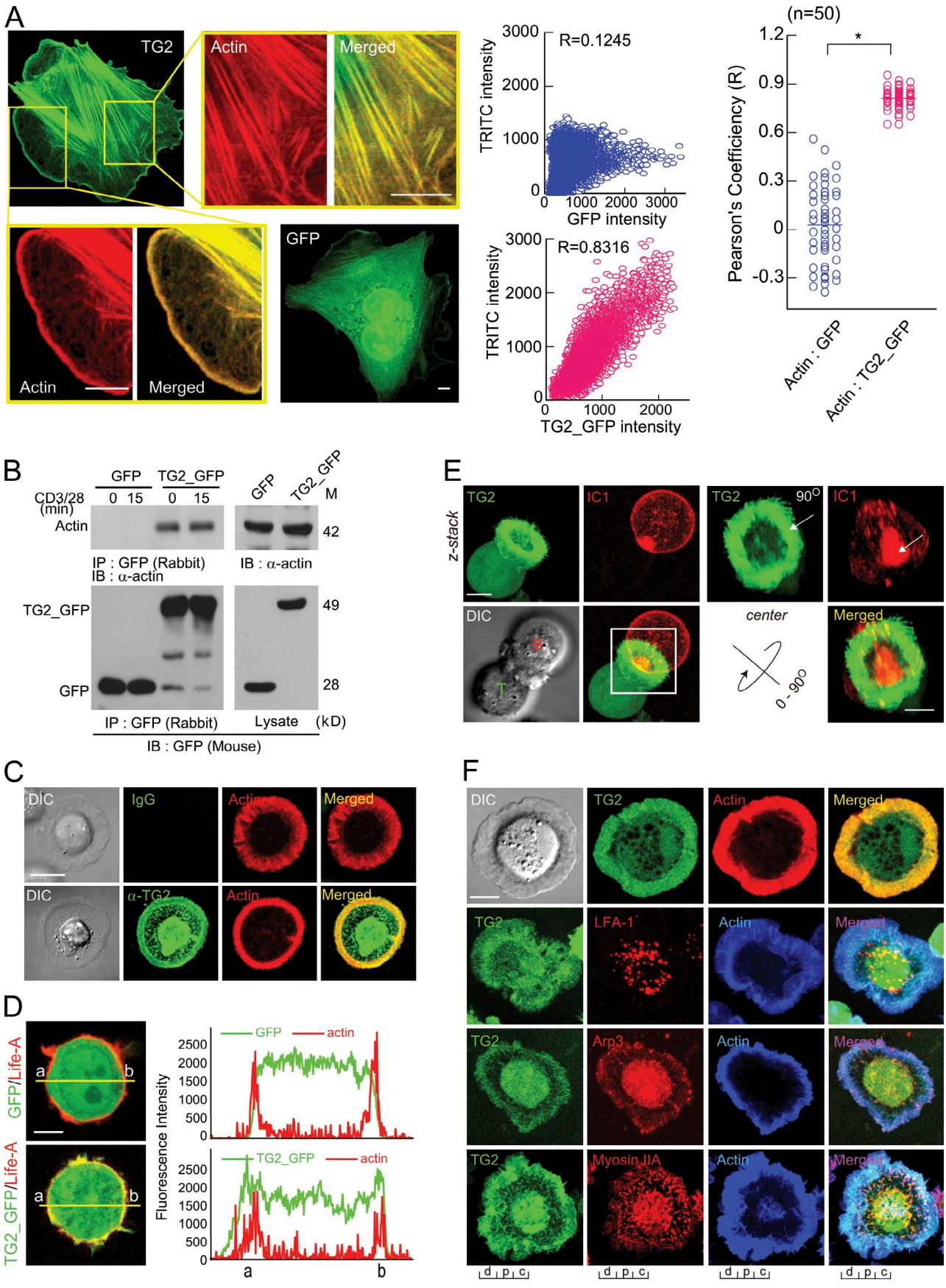

Figure 1. **TAGLN2 is associated with F-actin and localizes at the d-SMAC of IS in T cells.** (A) CHO-K1 cells transfected with TG2_GFP or GFP vector were stained with TRITC-phalloidin. The boxed areas (yellow) are represented as zoomed images in the right and bottom micrographs. (middle) The colocalization

characterized and functions by severing actin filaments and sequestering actin monomers. Depletion of cofilin results in the formation of increased and longer lamellipodial structures in T cells (Kim et al., 2014).

The structure of the actin network is also regulated through the actions of a variety of actin cross-linking or bundling proteins. An actin cross-linking protein, α-actinin, regulates IS formation (Gordón-Alonso et al., 2012). L-Plastin is involved in efficient spreading of T cells on surfaces with immobilized T cell receptor (TCR) ligands (Wang et al., 2010). Filamin A interacts with CD28 at the IS (Tavano et al., 2006). Overall, the studies on each of these proteins suggest that different actin regulators participate in different aspects of T cell activation and only a fully rearranged actin cytoskeleton is optimal for full T cell activation.

TAGLN (transgelin) family members have been identified as actin cross-linking/gelling proteins. The family comprises three isoforms, namely TAGLN1 (also known as transgelin1 or SM22α, highly expressed in smooth muscle cells; Camoretti-Mercado et al., 1998), TAGLN2 (also known as transgelin2 or SM22β, associated with various types of cancers; Zhang et al., 2002, 2010; Rho et al., 2009), and TAGLN3 (also known as transgelin3 or NP25, abundant in brain tissues; Mori et al., 2004). The term "transgelin" was originally derived from the transformation-sensitive and rapid actin-gelling properties of these proteins (Shapland et al., 1993). In this study, we found that TAGLN2 had a modest effect on actin cross-linking or bundling, whereas it substantially blocked depolymerization of and competed with cofilin to bind F-actin. These findings suggest that TAGLN2 has a unique role in actin reorganization, in addition to its previously reported function. Indeed, there is little information available regarding the role of actin-stabilizing proteins in IS formation and subsequent T cell activation.

Our study shows that TAGLN2 is the only transgelin isoform present in leukocytes, and it is segregated at the distal supramolecular activation cluster (SMAC; d-SMAC) within the IS after TCR stimulation. These results prompted us to explore the possibility of TAGLN2 as a potential regulator of IS formation and subsequent T cell activation. Through biochemical and genetic analyses, we uncovered evidence that TAGLN2 stabilizes the actin cytoskeleton, leading to an increase in F-actin content at the IS and subsequent activation of integrin function. *TAGLN2*$^{-/-}$ T cells are unable to sustain a conventional F-actin ring, thus decreasing cell adhesion and spreading after TCR stimulation. As a result, cytokine expression and effector function are impaired.

Results

TAGLN2 is highly expressed in immunogenic tissues and cells, and TAGLN2 knockdown reduces T cell activation

The calponin homology (CH) actin-binding domain is found in cytoskeletal and signal transduction proteins, including TAGLNs. A phylogenetic tree of the family of single CH domain-containing proteins is shown in Fig. S1 A. The TAGLN family, including TAGLN2, is evolutionarily related to Vav1 and IQGAP1, which are key cytoskeletal-regulatory proteins involved in T cell immunity.

The expressions of TAGLN1 and TAGLN3 are restricted to the smooth muscle (Camoretti-Mercado et al., 1998) and brain (Mori et al., 2004), respectively. However, the expression pattern of TAGLN2 has not yet been fully characterized. Thus, we first tested for the presence of *TAGLN2* in various human tissues by Northern blot analysis and observed high expression in the spleen (Fig. S1 B). Western blot and real-time quantitative PCR (qPCR) analyses of mouse tissues confirmed that TAGLN2 was most highly expressed in the thymus, spleen, and lymph nodes (Fig. S1 C). TAGLN2 expression was also detected in primary immune cells or immune cell lines, and we did not detect the presence of other TAGLNs in these cells (Fig. S1 D). The predominant expression of TAGLN2 in T cells prompted us to explore its role in cytoskeletal regulation, which is essential for T cell function. A dramatic reduction in *IL-2* mRNA and IL-2 protein levels was observed in human peripheral blood lymphocytes (PBLs) transfected with *TAGLN2* siRNA after stimulation with *Staphylococcal aureus* enterotoxin E (SEE)–pulsed Raji B cells (Fig. S1 E), suggesting a potential role for TAGLN2 in T cell immunity.

TAGLN2 binds to actin and localizes at the d-SMAC in the IS

Just like TAGLN1 and TAGLN3 (Camoretti-Mercado et al., 1998; Mori et al., 2004), TAGLN2 colocalized with actin stress fibers and also localized to the lamellipodial leading edge, where actin polymerization actively occurs in CHO-K1 cells (Fig. 1 A). Coimmunoprecipitation of actin with GFP-tagged TAGLN2 (TG2_GFP) before and after activation revealed that TAGLN2 binding to actin is stimulus independent (Fig. 1 B). These findings led us to analyze endogenous TAGLN2 localization in primary T cells. TAGLN2 was localized to the F-actin ring of mouse CD3$^+$ T cells loaded onto anti-CD3/28–coated

of GFP and TRITC signals was estimated by the Pearson's correlation coefficient (R). (right) R values of single cells are represented as single dots, and ≥50 cells were examined. Horizontal bars indicate the means. *, P < 0.05 versus GFP-transfected cells. (B) J-GFP and J-TG2_GFP cells were stimulated with anti-CD3/28. Samples were immunoprecipitated and blotted with antibodies against the indicated proteins. Data shown are representative of three independent experiments. IP, immunoprecipitation; IB, immunoblot; M, molecular mass. (C) Mouse CD3$^+$ T cells on anti-CD3/28 coverslips were stained for TG2 (rabbit IgG, negative control) and actin. (D) J-GFP and J-TG2_GFP cells transfected with LifeAct (Life-A) on PLL-coated coverslips were imaged and fluorescence intensity profiles were analyzed. Images and intensity profiles are representative of >50 cells. (E) J-TG2_GFP cells were conjugated for 30 min with SEE-Raji B cells (ICAM-1 [IC1]). 3D and rotating views of selected zoomed images (90°) of the boxed area are shown. Also refer to Video 1. Arrows indicate accumulation of TG2 and ICAM1 at the synapse site. (F) J-TG2_GFP cells on anti-CD3/28 coverslips were stained for LFA-1, Arp3, myosin IIA, and F-actin. Bottom images are shown, and each z-stack image is shown in Fig. S2. Also refer to Videos 2–4. c, central SMAC; p, peripheral SMAC; d, d-SMAC. All images are representative of >50 cells examined from three independent experiments. DIC, differential interference contrast. Bars, 10 µm.

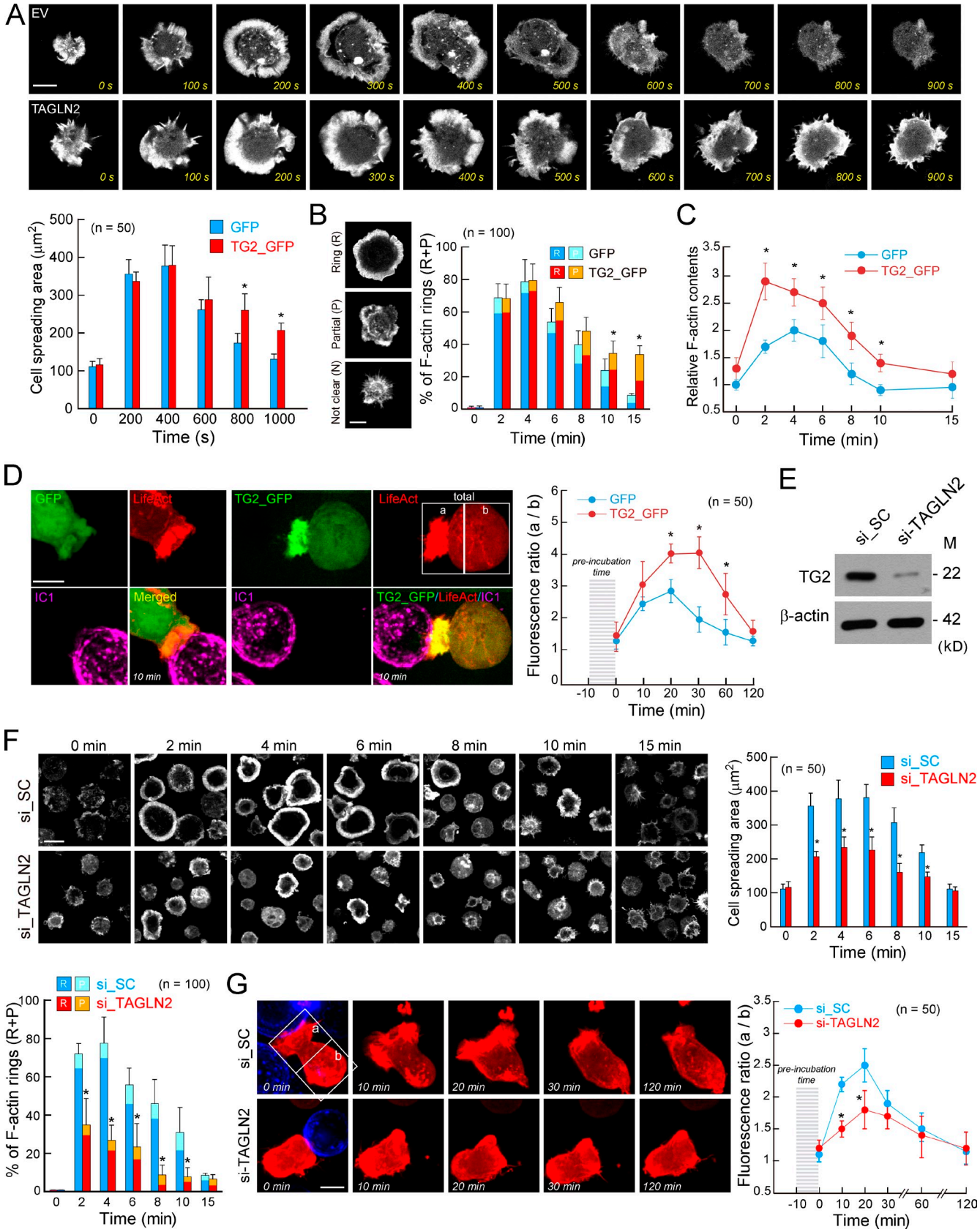

Figure 2. **TAGLN2 increases F-actin content and mediates long-lasting T cell adhesion and spreading.** (A) J-GFP and J-TG2_GFP cells transfected with LifeAct (white) were loaded on anti-CD3/28 coverslips. After initial contact, time-lapse images were acquired, and single images representing 100-s time points are shown. Also, refer to Videos 5 and 6. Cell spreading areas were measured using FLUOVIEW program. EV, empty vector. (B) Cells were loaded on anti-CD3/28 coverslips, incubated for the indicated time points, and stained for F-actin, and the percentages of F-actin rings were scored and quantified.

coverslips (Fig. 1 C). Ectopic overexpression of TG2_GFP in Jurkat T cells (J-TG2_GFP) revealed TG2_GFP expression not only in the cytoplasm but also in the membrane compartment (Fig. 1 D). Upon J-TG2_GFP cell conjugation with SEE-loaded Raji B cells, TG2_GFP localized to the outer border of ICAM-1, which is a representative peripheral SMAC molecule present on B cells (Fig. 1 E and Video 1). To examine the localization of TAGLN2 in greater detail, J-TG2_GFP cells were loaded on anti-CD3/28–coated coverslips, and then, the cells were fixed and stained with F-actin, LFA-1, Arp3, and myosin IIA. TAGLN2 was most clearly seen at the outer actin ring (d-SMAC; Fig. 1 F, d), although it was also observed in the nucleus (Fig. 1 F, Fig. S2, and Video 2). TG2_GFP signals strongly overlapped with Arp3 at the outer ring, but not with LFA-1 and myosin IIA, which are representative of the middle ring (peripheral SMAC; Fig. 1 F, p; Fig. S2; and Videos 3 and 4; Yi et al., 2012). Collectively, we concluded that TAGLN2 associates with F-actin and is a d-SMAC protein in the IS.

TAGLN2 controls the F-actin content in T cells

We next investigated the function of TAGLN2 in actin reorganization in Jurkat T cells. A kinetic study revealed that, although initial cell spreading and F-actin ring formation were similar, TAGLN2 overexpression prolonged the duration of T cell spreading and F-actin ring formation on anti-CD3/28–coated coverslips (Fig. 2, A and B; and Video 5 and 6). This was correlated with the up-regulation of total F-actin content in J-TG2_GFP cells after stimulation (Fig. 2 C). Accumulation of F-actin at the IS was also evident during T cell–APC conjugation. TG2_GFP was clearly overlapped with LifeAct (mCherry; Fig. 2 D, left), and the F-actin retention time at the contact region in J-TG2_GFP cells was longer than that of J-GFP cells (Fig. 2 D, right).

Conversely, targeted knockdown of *TAGLN2* by siRNA (Fig. 2 E) resulted in diminished cell spreading and F-actin ring formation (Fig. 2 F). Moreover, the F-actin retention time at the contact region was shorter than that of scrambled siRNA-transfected cells (Fig. 2 G). Collectively, these results demonstrate that TAGLN2 controls total F-actin content at the IS that subsequently influences F-actin ring formation and spreading.

TAGLN2 controls integrin-mediated T cell adhesion

Previous experiments have demonstrated that the actin cytoskeleton can regulate integrin-mediated T cell adhesion (Burn et al., 1988). Inhibitors such as cytochalasin B and D (Cyt D) have been used to inhibit β2- and β1-mediated adhesion to their ligands (Rothlein and Springer, 1986). Therefore, we explored whether prolonged accumulation of F-actin at the IS may reflect integrin activation. We performed a T cell–APC conjugation assay and found that J-TG2_GFP cells increased conjugate formation over time (Fig. 3 A). Strong inhibition of conjugate formation in J-TG2_GFP cells treated with Cyt D or TS1/18 (a blocking antibody for LFA-1) demonstrated that TAGLN2 controls LFA-1–mediated T cell adhesion to APC (Fig. 3 B). TAGLN2 overexpression did not change the expression levels of the cell surface molecules CD3, 28, LFA-1, or ICAM-1 (Fig. 3 C). An ICAM-1 adhesion assay further supported TAGLN2-mediated control of integrin function (Fig. 3 D). Conversely, TAGLN2 deficiency reduced conjugate formation (Fig. 3 E).

TAGLN2 directly binds to F-actin and weakly cross-links F-actin in bundles

To understand the mechanism of TAGLN2 involvement in actin assembly at the IS, we first analyzed TAGLN2 and actin interactions in vitro. We confirmed these interactions using a high-speed cosedimentation assay. TAGLN2 was recovered with F-actin in the pellet (Fig. 4 A), confirming the in vivo observation of association with stress fibers or localization at the lamellipodial leading edge. The binding of TAGLN2 to actin monomers was saturated at a 1:1 ratio ($B_{max} = 0.9175 \pm 0.102$ mol/mol), with a K_d of 7.395 μM (Fig. 4 B). TAGLN1 was reported to bundle actin filaments (Han et al., 2009); thus, we tested for a correlation between the bundling activity of TAGLN2 and the increase in the F-actin content of T cells. We found, by low speed centrifugation, that the well-known actin-bundling protein α-actinin (1 μM) precipitates most of the F-actin; however, TAGLN2 does not show any bundling activity up to a 1:2 ratio of actin to TAGLN2 (8 μM; Fig. 4 C). We saw bundling activity only at higher concentrations (16–24 μM), as assessed by low-speed centrifugation and EM (Fig. 4 D). In contrast to the strong, rope-like structure formed by α-actinin, TAGLN2-actin bundles were loosened, gel-like structures (Fig. 4 D). The optimal ratio of actin to common actin-bundling proteins such as fascin, fimbrin, filamin, and α-actinin is ∼1:0.05 to 1:0.5 (Glenney et al., 1981; Stokes and DeRosier, 1991; van der Flier and Sonnenberg, 2001; Gordón-Alonso et al., 2012). However, the requirement of exceptionally higher concentrations of TAGLN2 needed to cross-link actin implies that TAGLN2 has another function other than F-actin cross-linking.

TAGLN2 stabilizes F-actin and competes with cofilin for binding to F-actin

The aforementioned results prompted us to consider the other functions of TAGLN2 in actin reorganization. We performed

(left) Representative actin ring images were classified as ring (R), partial (P), and not cleared (N). (C) Cells were stimulated with soluble anti-CD3/28. At the indicated times, F-actin content was quantified using flow cytometry. The data are represented as relative fluorescence intensity compared with J-GFP cells at 0 min. (D) Cells were preincubated for 10 min with SEE-loaded Raji B cells (ICAM-1 [IC1]). The cells were then placed on PLL for the indicated time points. LifeAct redistribution was quantified as described in Materials and methods. (A–D) *, $P < 0.05$ versus J-GFP cells. (E–G) Jurkat T cells were transfected with either scrambled or siRNA targeting *TAGLN2* (70 nM). (E) After 48 h, TAGLN2 expression was determined by Western blot. M, molecular mass. (F) Cells were loaded on anti-CD3/28 coverslips for indicated time points and then stained with TRITC-phalloidin. Cell spreading area and F-actin rings were analyzed as in B. (G) LifeAct redistribution at the IS was determined as in D. Graphical data shown are means of three experiments ± SD, with >50 cells. (F and G) *, $P < 0.05$ versus scrambled siRNA (si_SC). Bars, 10 μm.

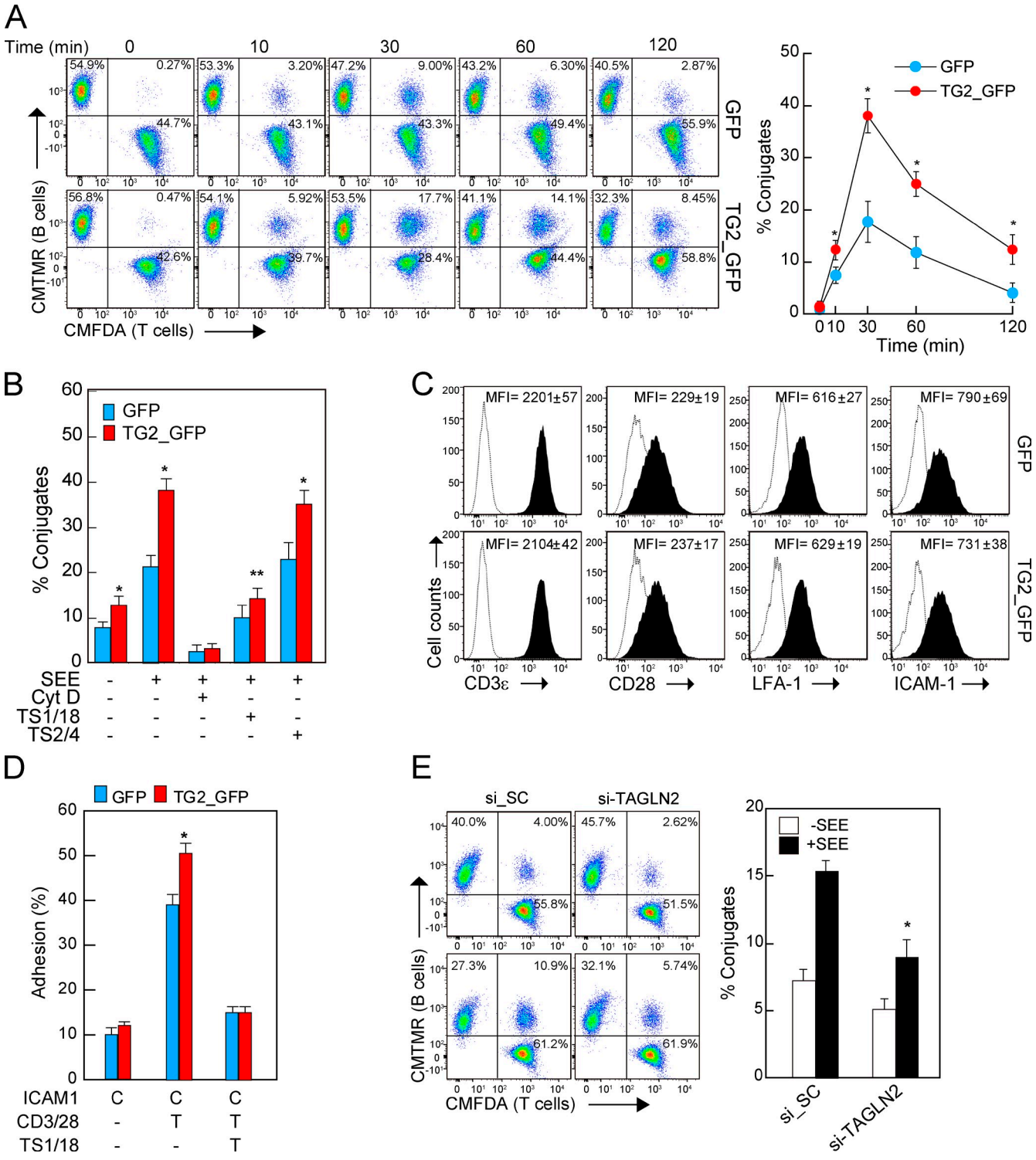

Figure 3. **TAGLN2 controls T cell adhesion through integrin activation.** (A) Representative flow cytometric profiles of conjugate formation between J-GFP or J-TG2_GFP cells and Raji B cells at indicated time points. The percentages of conjugates were calculated as described in Materials and methods. (B) J-GFP and J-TG2_GFP cells were pretreated for 30 min with or without 2 µM Cyt D, 10 µg/ml TS1/18, and 10 µg/ml TS2/4, and then, the cells were incubated for 30 min with SEE-Raji B cells. *, $P < 0.05$ versus J-GFP in each experimental condition. **, $P < 0.05$ versus J-TG2_GFP cells with SEE-loaded Raji B cells. (C) Surface expression of CD3-ε, CD28, LFA-1, and ICAM-1. Mean fluorescence intensity (MFI) of whole cell population is shown in each graph. Empty line, isotype control. (D) J-GFP and J-TG2_GFP were preincubated for 30 min with or without 10 µg/ml TS1/18 and were then applied to human ICAM-1-Fc coverslips for 30 min with or without anti-CD3/28 stimulation. Adherent cells were detected using a fluorescence plate reader. C, coated; T, treated. *, $P < 0.05$ versus anti-CD3/28–stimulated J-GFP cells. (E) Cells from Fig. 2 E were mixed with SEE-Raji B cells, and the percentages of conjugates were determined as in A. Flow cytometric plots shown are representative of three independent experiments, and results are the mean ± SD of triplicate experiments. *, $P < 0.05$ versus scrambled siRNA (si_SC) in the presence of SEE.

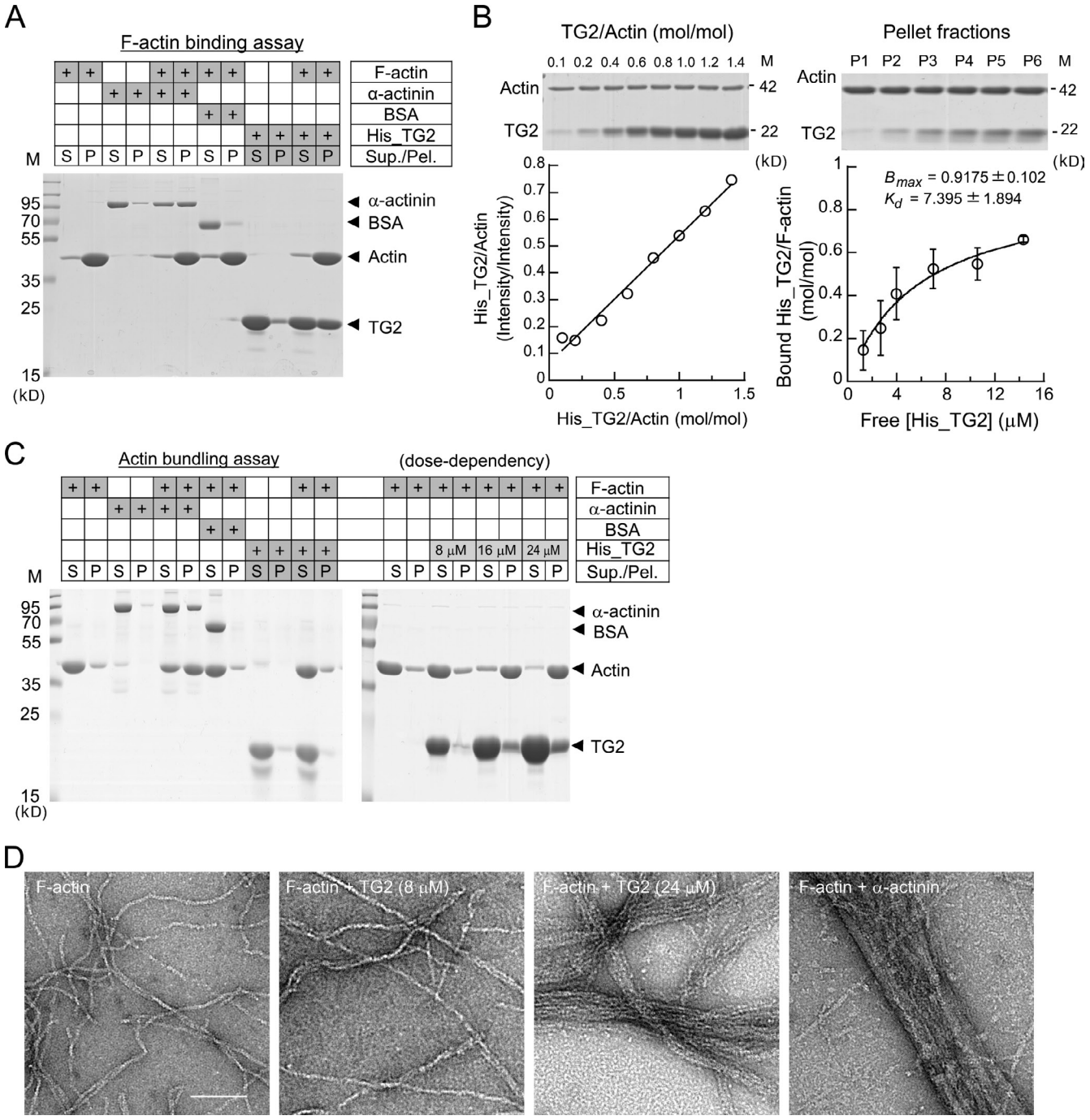

Figure 4. **TAGLN2 directly binds to F-actin and weakly cross-links actin in bundles.** (A) Actin was polymerized in APB and then incubated for 30 min with 8 μM TAGLN2, 1 μM α-actinin, and 1 μM BSA. After high-speed centrifugation (100,000 *g*), pellets were separated from supernatants and analyzed by SDS-PAGE. S, supernatant; P, pellet. (B) To generate standard curves, different amounts of actin (4 μM) and TAGLN2 (0.4–5.6 μM) were loaded on an SDS-PAGE gel, and the intensities of the bands were measured by a densitometer. The actin binding affinity was measured as described in the Materials and methods. (C) For actin bundling assay, various doses of TAGLN2 (8–24 μM) were incubated with F-actin (4 μM). After low-speed centrifugation (10,000 *g*), pellets and supernatants of the samples were analyzed. All data shown are representative of three independent experiments. M, molecular mass. (D) The reactants above C were examined via EM. Images shown are representative of three independent experiments. Bar, 100 nm.

an actin polymerization assay with pyrene-labeled actin and compared the polymerizing activity of TAGLN2 with that of Arp2/3 and/or the VCA (verprolin-homology, cofilin homology, and acidic) domain of neuronal WASp (Blanchoin et al., 2000). Although Arp2/3 and VCA successfully enhanced spontaneous polymerization under actin polymerization buffer (APB), TAGLN2 slightly reduced the kinetics of spontaneous actin polymerization (Fig. 5 A). We also measured the concentration of globular actin (G-actin) required for polymerization (critical concentration) in the presence or absence of TAGLN2 and found that addition of TAGLN2 does not change the critical concentration of G-actin (Fig. 5 B).

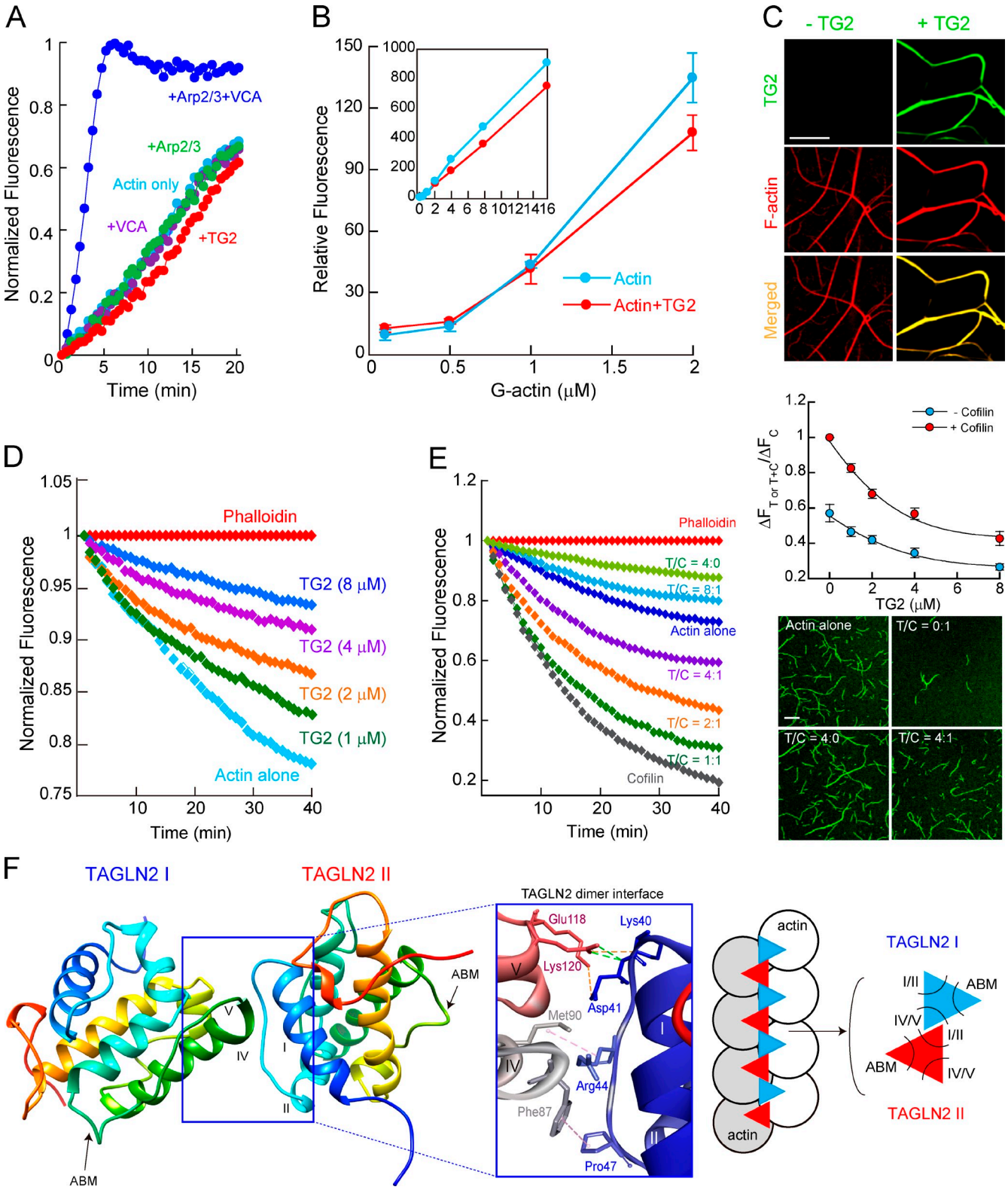

Figure 5. **TAGLN2 stabilizes F-actin and competes with cofilin for binding to F-actin.** (A) Actin polymerization was performed with pyrene-labeled 4 μM G-actin in APB containing 10 nM Arp2/3, 400 nM VCA, 4 μM TAGLN2, or Arp2/3 + VCA. The extent of polymerization is shown in normalized fluorescence units. (B) Pyrene-labeled G-actin was diluted to various concentrations in the presence or absence of an equimolar concentration of TAGLN2, and fluorescence was measured 4 h after adding APB to initiate polymerization. Inset graph indicates fluorescence intensities of 0–16μM pyrene-labeled G-actin mixed with same molar concentration of TAGLN2. (C) To visualize TAGLN2 and F-actin, G-actin was incubated for 1 h in APB in the presence or absence of TAGLN2 conjugated with Dylight 488. F-actin was stained with TRITC-phalloidin. (D) Depolymerization of actin filaments was performed in the presence of various concentrations of TAGLN2. 4 μM phalloidin was used as a positive control. Actin was polymerized in the presence of TAGLN2 or phalloidin for 1 h in APB and then diluted fivefold into G buffer to initiate depolymerization. The degree of depolymerization was monitored using a fluorometer. (E) Actin depolymerization was performed as in D in the presence or absence of 1 μM cofilin. T/C indicates the molar ratio of TAGLN2 (T)

The binding of fluorescently labeled TAGLN2 along actin filaments (Fig. 5 C) led us to examine whether TAGLN2 may be involved in F-actin stabilization as a side-binding protein. TAGLN2 blocked spontaneous actin depolymerization in concentrations ranging from 1 to 8 µM, which were lower than those needed for bundling (Fig. 5 D). This demonstrated that TAGLN2 stabilizes F-actin. Moreover, TAGLN2 blocked cofilin-mediated depolymerization, as determined by a depolymerization assay and confocal analysis (Fig. 5 E).

The crystal structure of TAGLN1 was reported to contain two cross-linked monomers of TAGLN1 (Li et al., 2008). Using the TAGLN1 homodimer as a template, we predicted the dimerization of TAGLN2 monomers (Fig. 5 F). Interestingly, we found a similar mode of homodimerization for TAGLN2. It was mediated by amino acids at the binding interface that correspond to those of the TAGLN1 homodimer (Li et al., 2008). The structure of the homodimeric TAGLN2 model enabled us to predict an underlying mechanism of TAGLN2 action in F-actin stabilization. As shown schematically in Fig. 5 F, dimerization of TAGLN2 monomers, through the interaction of one side of the first monomer (helix I and II) with the other side of second monomer (helix IV and V), can generate multimers of TAGLN2 that stabilize an incoming actin molecule's position on the growing F-actin lining. The 1:1 stoichiometry of TAGLN2 to actin also suggests that there is only one actin-binding motif (ABM) on each TAGLN2 monomer (Fig. 4 B). These observations suggest a model in which TAGLN2 functions as a "molecular staple" on polymerized actin, binding to actin at one end (fulcrum) and undergoing multimeric interactions with two arms (Fig. 5 F, right).

The ABM is required for TAGLN2-mediated T cell activation

Sequence alignment with TAGLN1 and TAGLN3 revealed that TAGLN2 contains a predicted ABM between residues 153 and 160. Deletion of amino acids 153–160 (ΔABM) reduced TAGLN2 association with F-actin (Fig. 6, A and B). This mutant also lost actin-stabilizing activity (Fig. 6 C), further corroborating that the actin stabilizing activity of TAGLN2 is fully dependent on its binding to F-actin. To investigate whether TAGLN2 involvement in T cell activation is related to its binding to actin, we also generated J-TG2ΔABM_GFP cells (Fig. 6 D). We observed diminished accumulation of TAGLN2 at the IS, and the expression of *IL-2* mRNA was attenuated in these cells compared with J-TG2_GFP cells (Fig. 6, D and E). These cells also failed to increase conjugate formation (Fig. 6 F). We questioned whether T cell activation by TAGLN2 is caused by its primary role in actin signaling or a secondary effect stemming from increased conjugate formation. To test this, J-GFP, J-TG2_GFP, or J-TG2ΔABM_GFP cells were loaded on anti-CD3/28–coated plates with or without ICAM-1 (±ICAM-1), and IL-2 production was measured. J-TG2_GFP cells on the anti-CD3/28+ICAM-1–coated plates produced the most IL-2. This suggested that TAGLN2 function is enhanced by integrin LFA-1 binding to its ligand ICAM-1 (Fig. 6 G). On anti-CD3/28–coated plates, however, production of IL-2 in J-TG2_GFP cells was also increased when compared with J-GFP or J-TG2ΔABM_GFP cells (Fig. 6 G). This suggests that the primary role of TAGLN2 in regulation of actin is essential for TAGLN2-mediated T cell function.

TAGLN2 knockout leads to diminished F-actin content and F-actin ring formation—resulting in lowered cell spreading—and shows attenuated cofilin activity in vivo

To connect the in vitro and in vivo data, we generated mice deficient in *TAGLN2* (Fig. S3, A and B). The sizes of primary and secondary lymphoid organs were not changed, and the weights of age-matched littermates also did not differ significantly among wild-type (WT; +/+), heterozygous (+/−), and TAGLN2-null (−/−) mice (Fig. S3, C and D). The absence of TAGLN2 expression was confirmed using Western blotting (Fig. S3 E). The *TAGLN2*$^{-/-}$ mice showed normal T cell development, in terms of the number and percentage of CD4$^+$ and CD8$^+$ single-positive cells in the thymus, lymph nodes, and spleen (Fig. S3 F), as well as normal B cell and dendritic cell populations in the spleen (Fig. S3 G). CD3$^+$ T cells showed normal surface expression of CD3-ε and CD28 (Fig. S3 H). Response to lipopolysaccharide was not significantly altered in either dendritic cells (DCs; Fig. S3 I) or B cells (Fig. S3 J) taken from *TAGLN2*$^{-/-}$ mice.

We also generated transgenic mice by using an Lck (lymphocyte-specific protein tyrosine kinase) promoter-based vector containing GFP or TG2_GFP, and we verified the GFP signals within well-defined T cell regions in lymphoid organs such as the thymus, spleen, and lymph nodes (Fig. S4 A). The expression levels of GFP and TG2_GFP were confirmed (Fig. S4 B). The mice exhibited normal T cell development as determined by the ratio of CD4$^+$/CD8$^+$ cells (Fig. S4 C).

We compared cell spreading and F-actin ring formation in CD3$^+$ T cells purified from *TAGLN2*$^{+/+}$ and *TAGLN2*$^{-/-}$ mice before and after stimulation on anti-CD3/28–coated coverslips. A kinetic study revealed that the TAGLN2 deficiency inhibited cell spreading as well as diminished F-actin ring formation (Fig. 7 A). These cells showed a reduction in total F-actin content after T cell stimulation (Fig. 7 B). *TAGLN2*$^{-/-}$ CD3$^+$ T cells showed a significant reduction of conjugate formation with SEE-loaded CD19$^+$ B cells purified from WT mice (Fig. 7 C). The ability to adhere to ICAM-1 was also diminished in these cells, suggesting weakened LFA-1 function (Fig. 7 D).

We next examined the relationship between TAGLN2 and cofilin in vivo. Because active cofilin functions to rapidly disassemble F-actin, we tested the ability of TAGLN2 to

and cofilin (C) in the reaction. (top) Total change in pyrene intensities (ΔF) were calculated as described in Materials and methods. Results represent means ± SD of triplicate experiments. For confocal image analysis, pyrene-labeled G-actin was replaced with 488–G-actin. All data shown are representative of at least three independent experiments. (F) Prediction of the ribbon structure of a TAGLN2 homodimer using Chimera software. (left) Black arrows indicate the actin-binding motif (ABM). (right) TAGLN2 dimer and multimers are shown schematically. The TAGLN2 dimer is represented by triangular monomers with helices I and II, helices IV and V, and ABM at the three vertices represented by arcs. Bars, 5 µm.

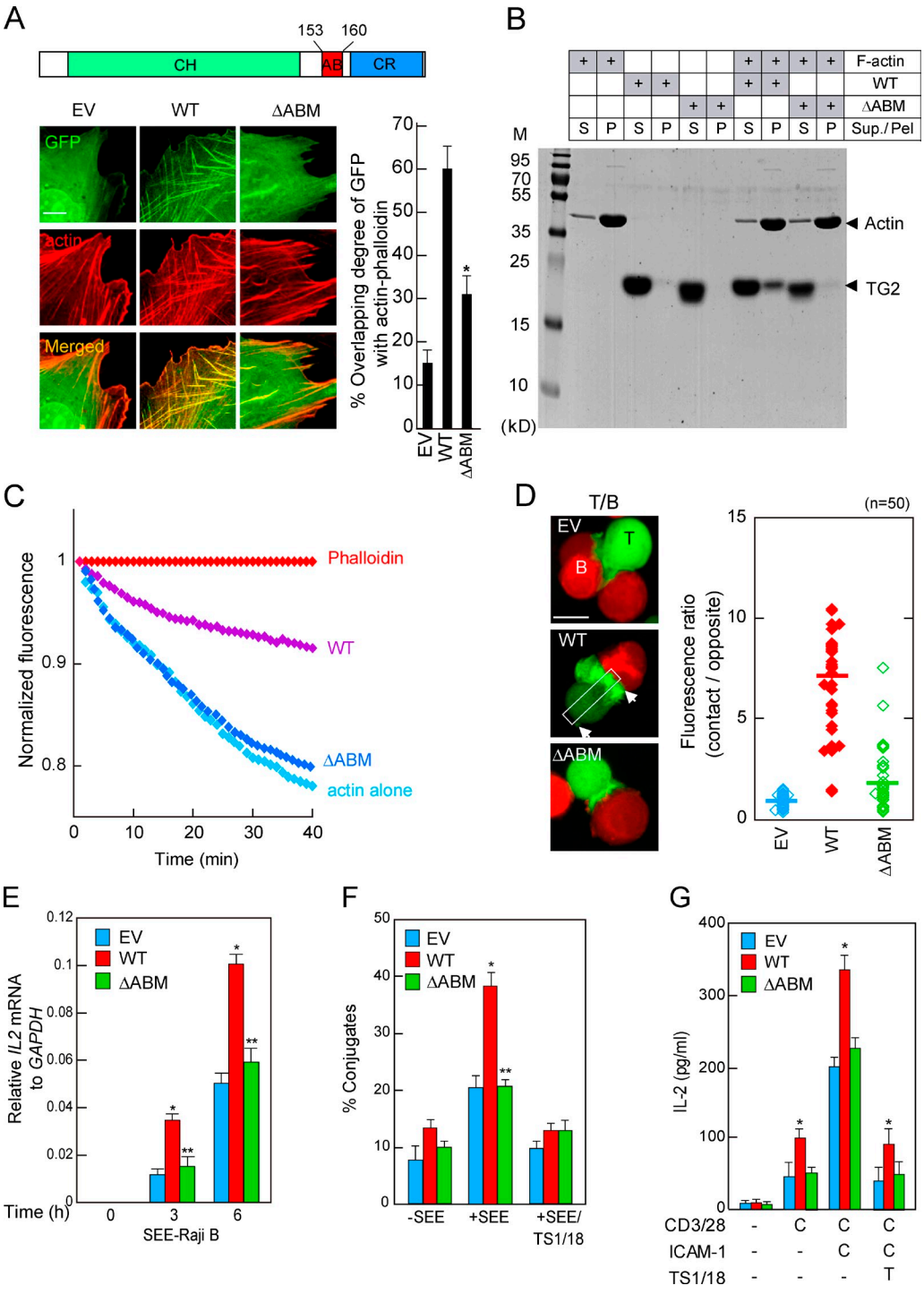

Figure 6. **Mutation at actin binding site loses functions of F-actin stabilization and T cell activation.** (A) Schematic diagram of wild type (WT)–TG2 and TG2ΔABM. CH, calponin homology; ABM, actin-binding motif; CR, calponin repeat. CHO-KI cells transfected with WT-TG2_GFP or TG2ΔABM_GFP were stained for F-actin (TRITC-phalloidin), and colocalization between GFP and TRITC was calculated with the FLUOVIEW and represented as a percentage (bottom). Images are representative of >50 cells examined. Results represent means ± SD of triplicate experiments. *, P < 0.05 compared with cells expressing WT-TG2. EV, empty vector. (B and C) F-actin binding (B) and actin depolymerization (C) assays were performed as described in Fig. 4 A and Fig. 5 D. Data shown are representative of three independent experiments. M, molecular mass; S, supernatant; P, pellet. (D) J-GFP, J-TG2_GFP, and J-TG2ΔABM_GFP were incubated with SEE-loaded Raji B cells for 30 min. (left) The arrows indicate the accumulation of GFP signals at the IS. The ratio of contact/opposite fluorescence was calculated. The ratio of contact/opposite fluorescence in the white boxed area was calculated. Each dot represents 50 cells examined. Horizontal bars indicate the mean of fluorescence intensities. Data shown are representative of three independent experiments. T, J-GFP, J-TG2_GFP, and J-TG2ΔABM_GFP cells; B, Raji B cells. (E) *IL2* mRNA levels were measured using real-time quantitative RT-PCR. (F) Conjugate formations were determined as described in Fig. 3. (G) IL-2 secretions in each condition were assessed by ELISA. Results are the means ± SD of triplicate experiments. *, P < 0.05 versus J-GFP; **, P < 0.05 versus J-TG2_GFP. T, TAGLN2; C, cofilin. Bars, 10 µm.

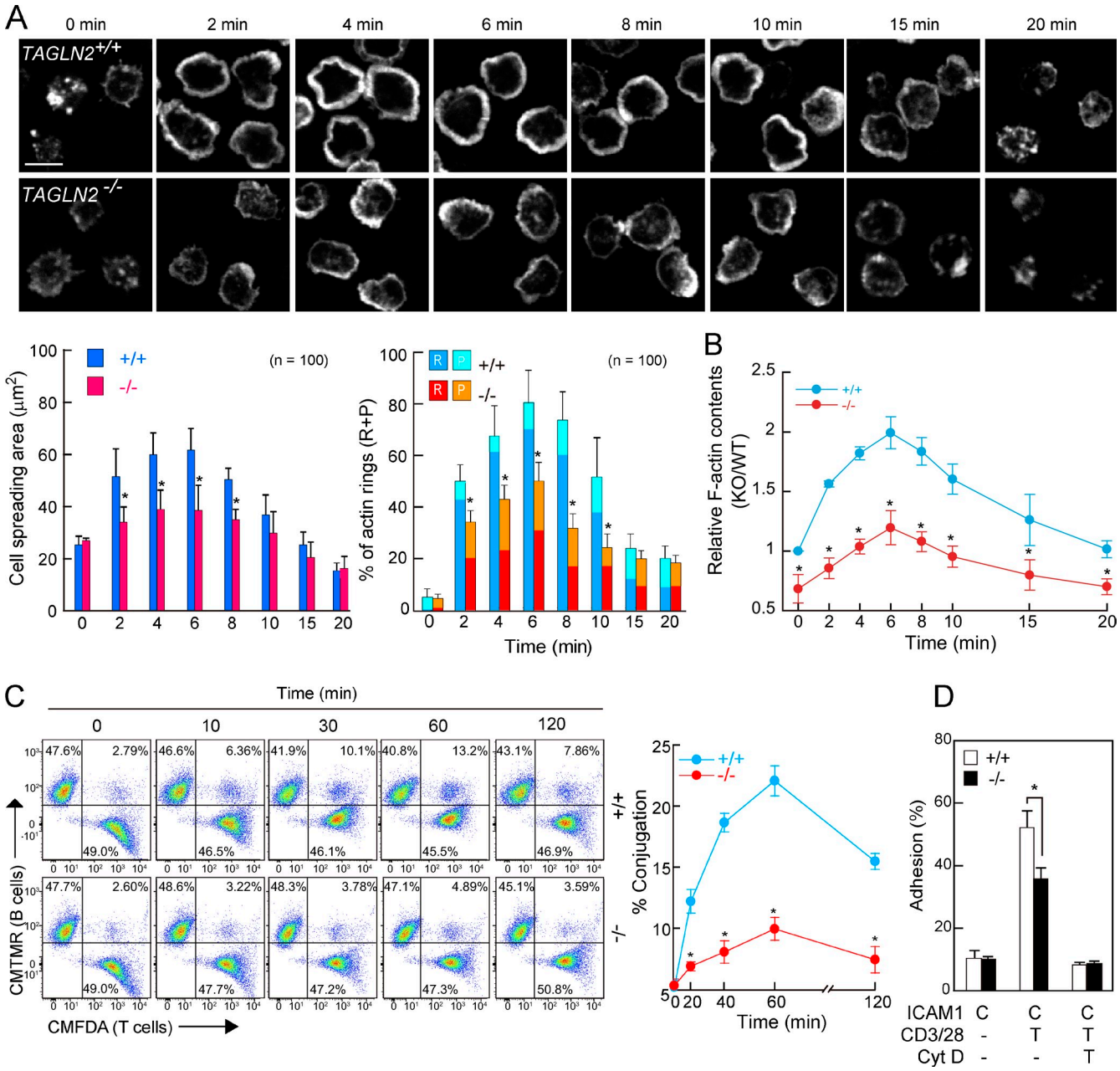

Figure 7. **A TAGLN2 knockout leads to diminished F-actin content and F-actin ring formation, resulting in lowered cell spreading and LFA-1–mediated conjugation formation.** (A) T cells from *TAGLN2*$^{+/+}$ and *TAGLN2*$^{-/-}$ mice were loaded on anti-CD3/28–coated coverslips for the indicated time points. Images shown are representative of three independent experiments. Cell spreading area and the percentages of actin rings were measured, as shown in Fig. 2 (A and B). R, ring; P, partial. Bar, 10 μm. (B) Relative F-actin content was measured as in Fig. 2 C. KO, knockout. (C) Mouse CD3$^+$ T cells were mixed with SEB-loaded B cells, and conjugate formation for the indicated time points was determined as in Fig. 3 A. (D) BCECF-labeled mouse CD3$^+$ T cells were preincubated for 30 min with or without 2 μM Cyt D, and then, adhesion to mICAM-1Fc in response to anti-CD3/28 was determined by measuring fluorescence intensity. All graphical results represent means ± SD of triplicate experiments. *, $P < 0.05$. T, TAGLN2; C, cofilin.

overcome cofilin-mediated actin depolymerization in CHO-K1 cells. We generated an active form of cofilin by substitution of Ser-3 to Ala-3 (cofilin/S3A; Moriyama et al., 1996). Overexpression of TAGLN2 markedly protected F-actin within stress fibers from cofilin-mediated destruction, whereas the actin-binding mutant (ΔABM) had little effect (Fig. 8 A). In Jurkat T cells, cofilin/S3A led to impaired spreading (area) on anti-CD3/28–coated plates, presumably as a result of the excessive depolymerization of F-actin (Fig. 8 B and Video 7). However, cotransfection with WT-TG2, but not TG2ΔABM, blocked the cofilin effect (Fig. 8 B), thereby corroborating that TAGLN2 antagonizes cofilin activity in vivo as it does in vitro. Cofilin almost similarly colocalized with TAGLN2 (Fig. 8 B and Video 8). Surprisingly, however, careful examination revealed that cofilin mainly localized at two distinguishable regions in the IS—the central SMAC (corresponding to the "F-actin hole") and upper region of d-SMAC—where TAGLN2 is rather excluded (Fig. 8 C), suggesting specific locations of two proteins for opposite functions in the IS.

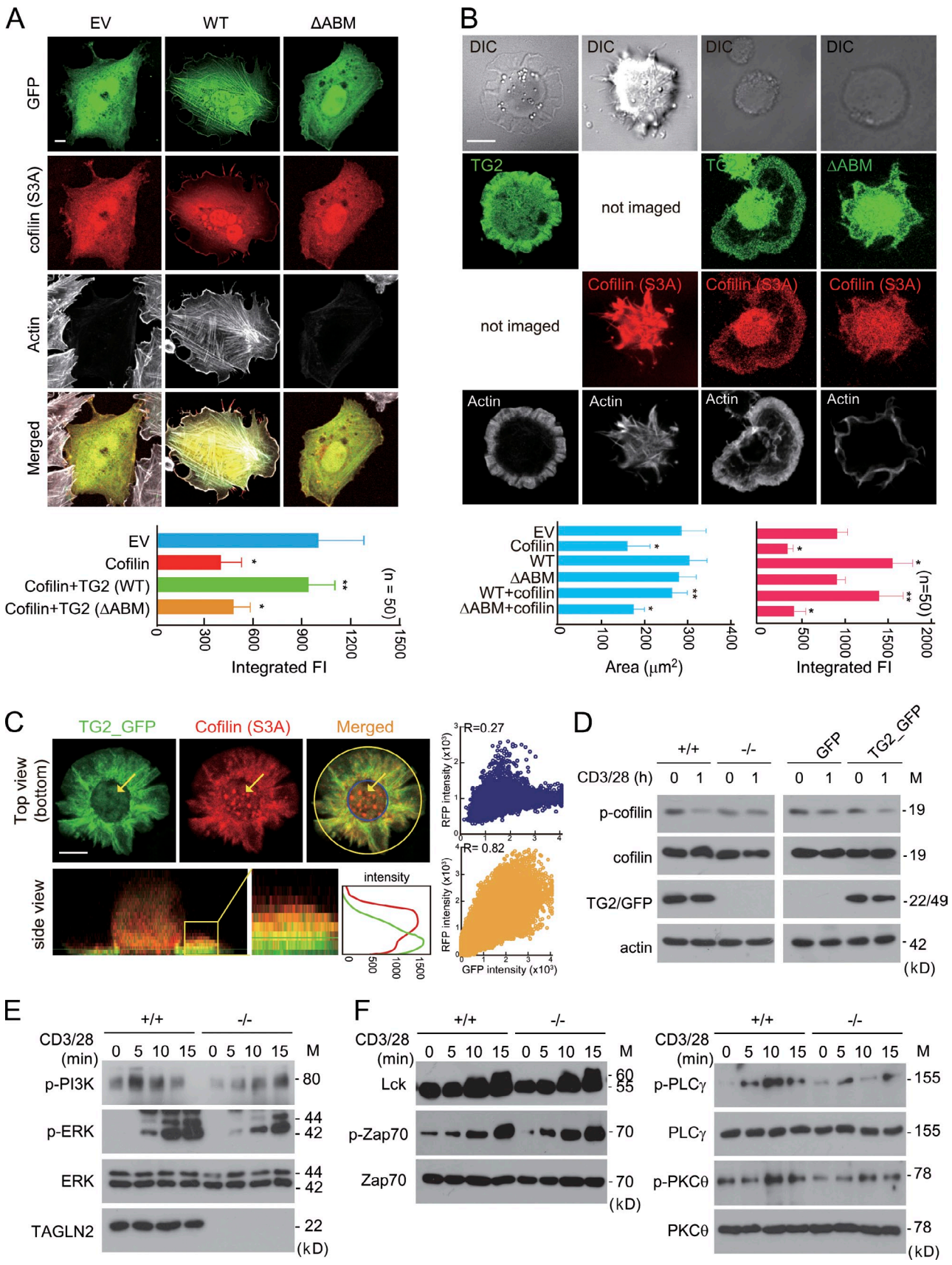

Figure 8. **TAGLN2 antagonizes cofilin in vivo, and TAGLN2$^{-/-}$ T cells show substantial retardation of cofilin activity upon TCR stimulation.** (A) CHO-K1 cells were transfected with the indicated constructs and then stained with Alexa Fluor 647–phalloidin. The integrated fluorescence (FI) of F-actin in each transfected cell was estimated by FLUOVIEW. (B) Jurkat T cells were cotransfected with the indicated constructs. Cells were loaded on anti-CD3/28–coated

Although most studies have associated cofilin activation with F-actin depolymerization, this relationship does not always hold. Indeed, cofilin activity favors F-actin polymerization via its actin-severing activity in vivo and is therefore known to positively regulate T cell activation (Samstag et al., 2003). If this is the case, there must be signaling cross talk or a cooperative function, but not opposition, between TAGLN2 and cofilin in vivo. Interestingly, we found that the dephosphorylation (activation) of cofilin was not obvious in *TAGLN2*$^{-/-}$ CD3$^+$ T cells after anti-CD3/28 stimulation, whereas the total amount of cofilin was similar in both types of T cells (Fig. 8 D). The opposite of this effect was also seen in transgenic TG2_GFP CD3$^+$ T cells (Fig. 8 D). In addition, we observed reduced phosphorylation of phosphoinositide 3-kinase (PI3K) and extracellular signal–regulated kinase (ERK), an upstream Ras-signaling cascade of cofilin dephosphorylation (Wabnitz et al., 2006), in *TAGLN2*$^{-/-}$ CD3$^+$ T cells (Fig. 8 E).

TCR triggering leads to proximal and distal intracellular signaling events that are related to actin dynamics. As shown in Fig. 8 F, none of the proximal molecules showed impaired phosphorylation after TCR stimulation in *TAGLN2*$^{-/-}$ CD3$^+$ T cells. This could be explained by the fact that none of these signaling molecules require actin for recruitment to the IS (Larghi et al., 2013). On the other hand, the phosphorylation of PLC-γ was attenuated in *TAGLN2*$^{-/-}$ CD3$^+$ T cells (Fig. 8 F). This impairment attenuated distal signaling by reducing PKC-θ and ERK activation (Fig. 8 F). PLC-γ phosphorylation depends not only on recruitment to the IS but also on correct spatial organization, driven by F-actin polymerization and retrograde flow (Babich et al., 2012). These results suggest that TAGLN2 plays a role in the spatial organization of IS, which is essential to maintain signaling activation.

TAGLN2 positively regulates T cell activation

Finally, we examined the physiological significance of TAGLN2 in T cell immunity. CD3$^+$ T cells from *TAGLN2*$^{-/-}$ mice showed decreased secretion of IL-2 after incubation with the *S. aureus* enterotoxin B (SEB)–loaded CD19$^+$ B cells or stimulation with anti-CD3/28 antibodies (Fig. 9 A). To evaluate more antigen-specific effector functions, we generated *OTII TCR*$^+$ and *OTI TCR*$^+$ mice with or without *TAGLN2* gene. Purified CD4$^+$ or CD8$^+$ T cells from *OTII TCR*$^+$/*TAGLN2*$^{-/-}$ and *OTI TCR*$^+$/*TAGLN2*$^{-/-}$ mice, respectively, showed a significant reduction of IFN-γ and IL-2 protein levels (Fig. 9 B) along with the decreased proliferation in response to the specific ovalbumin (OVA) peptides (Fig. 9 C). Conversely, CD3$^+$, CD4$^+$, and CD8$^+$ T cells from transgenic mice with TG2_GFP exhibited approximately a twofold increase in IL-2 or IFN-γ expression in response to the indicated stimuli (Fig. S4, D–F).

We next assessed the ability of CD8$^+$ T cells to kill target cells. *TAGLN2*$^{-/-}$ CD8$^+$ T cells exhibited a profound decrease in target cell lysis (Fig. 9 D). Flow cytometric analysis of *TAGLN2*$^{-/-}$ CD8$^+$ T cells showed reduced expression of lytic granules (granzyme B and perforin) after stimulation (Fig. 9 E), along with the consistent reduction in the secretion of mature granzyme B (Fig. 9 F). On the other hand, CD8$^+$ T cells also showed a reduced conjugation to target cells (Fig. 9 G). These results suggest that decreased cytotoxicity of *TAGLN2*$^{-/-}$ CD8$^+$ T cells is resulted from both reduced expression of lytic granules and weakened adhesion to target cells.

To further confirm that defects in the actin-binding ability of TAGLN2 also affect T cell spreading and activation in vivo, we performed retroviral transduction/reconstitution experiments in *TAGLN2*$^{-/-}$ T cells. In contrast to WT cells, TG2ΔABM cells did not properly form F-actin rings when reconstituted cells were loaded on anti-CD3/28–coated coverslips (Fig. 9 H). Moreover, the mutant failed to mediate normal T cell activation when the reconstituted cells were incubated with SEB-loaded CD19$^+$ B cells (Fig. 9 I). To further determine whether the signaling defects in *TAGLN2* knockouts are a direct result of TAGLN2 function on F-actin polymerization, or a secondary defect in integrin-mediated cell adhesion, the reconstituted cells were loaded on anti-CD3/28–coated plates with or without ICAM-1 (±ICAM-1), and intracellular signaling was examined. In contrast to the *TAGLN2*$^{+/+}$ or WT-transduced *TAGLN2*$^{-/-}$ T cells, ΔABM-transduced T cells were not optimally phosphorylated in either condition (±ICAM-1; Fig. 9 J). These results strongly suggested that direct modulation of actin reorganization is most critical for TAGLN2 function and that integrin-mediated adhesion is important.

Discussion

Once the IS is established, the surface of the distal region is enriched in molecules with large extracellular domains, such as CD43 and CD45 (Delon et al., 2001; Freiberg et al., 2002), whereas a stable centripetal retrograde actin flow drives and regulates T cell activation in the cytoplasmic region (Babich et al., 2012). To meet the needs of spatial and temporal regulation in the IS, actin polymerization and depolymerization are tightly regulated by many accessory proteins like Arp2/3, WASp, WAVE, cofilin, and HS12 (Huang and Burkhardt, 2007). We have found that another actin binding protein, TAGLN2, colocalizes with F-actin in d-SMAC and controls F-actin levels at the IS by stabilizing F-actin and in part antagonizing cofilin-mediated

coverslips for 5 min, fixed, and stained with Alexa Fluor 647–phalloidin. Images are representative of >50 cells examined. The areas and fluorescence intensity of F-actin were analyzed by FLUOVIEW. Data are means ± SD of triplicate experiments. (A and B) *, P < 0.05 versus empty vector (EV). **, P < 0.05 versus cofilin alone. (C) Live images of TG2_GFP and cofilin/S3A_RFP were acquired from cells in B. The colocalization (yellow and blue circles) was estimated as described in Fig. 1 A. The yellow arrows indicate the F-actin hole. The boxed area (yellow) is represented as 4× zoomed images in the right and quantitated by fluorescence intensity. Data are representative of >50 cells examined. (D–F) Indicated CD3$^+$ T cells were stimulated with an anti-CD3/28 for the indicated time points. (D) The phosphorylated and total forms of cofilin were assessed by Western blotting. The phosphorylated and total forms of PI3K and ERK (E), Lck, Zap70, PLC-γ, and PKC-θ (F) were also detected by Western blotting. The data are representative of three independent experiments. DIC, differential interference contrast; M, molecular mass. Bars, 10 µm.

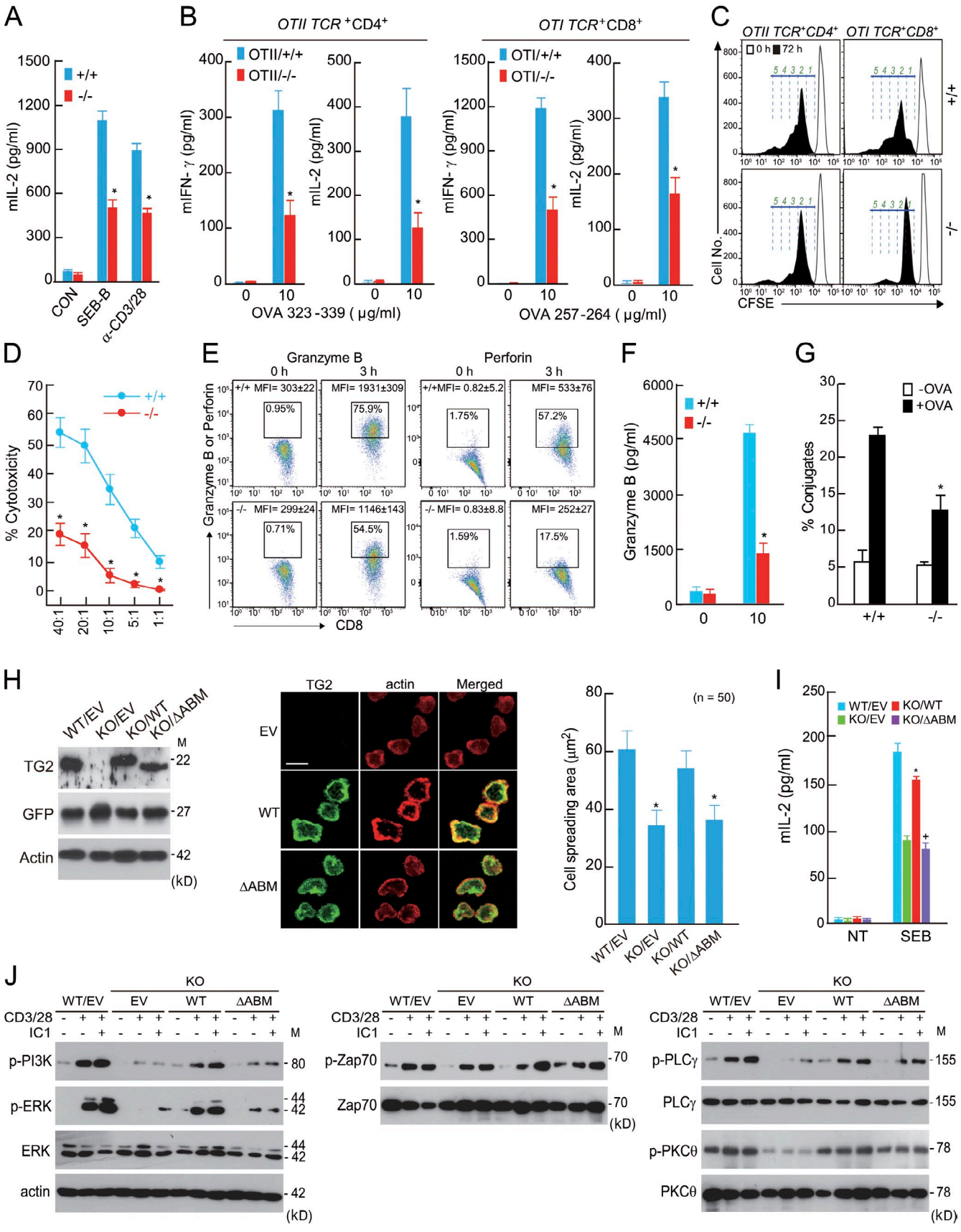

Figure 9. **TAGLN2 is necessary for effector T cell function.** (A) CD3+ T cells from *TAGLN2*$^{+/+}$ and *TAGLN2*$^{-/-}$ mice were stimulated with anti-CD3/28 or incubated with SEB-pulsed CD19+ B cells for 24 h, and the levels of IL-2 production were measured using ELISA. CON, control. (B) *OTII TCR*+ CD4+ or *OTI TCR*+ CD8+ T cells from *TAGLN2*$^{+/+}$ and *TAGLN2*$^{-/-}$ mice were stimulated with or without OVA-loaded DCs for 24 h. IFN-γ and IL-2 in the supernatant were

disassembly. This function is also connected to the up-regulation of LFA-1 activity in T cells. Furthermore, transgenic or knockout T cells showed up-regulated or impaired activation, demonstrating that TAGLN2 is an important actin regulator in T cells.

The similarities between TAGLN2 and its other two family members, TAGLN1 and TAGLN3, indicate actin-bundling or -gelling functions (Shapland et al., 1993; Han et al., 2009); however, we detected actin bundling effects only at exceptionally high concentrations of TAGLN2 (four to eightfold greater than actin). Because most actin-bundling proteins can optimally cross-link actin into bundles at concentrations 2–20-fold lower than actin (Glenney et al., 1981; Stokes and DeRosier, 1991; van der Flier and Sonnenberg, 2001; Gordón-Alonso et al., 2012), it is unlikely that TAGLN2-actin bundling is related to its biological function under physiological conditions. Instead, we found that TAGLN2 could stabilize and protect F-actin from cofilin-mediated depolymerization, which was also confirmed by confocal microscopy. The inability of the actin-binding mutant to protect F-actin and to enhance T cell activation suggests that TAGLN2 function is dependent on binding to actin. The mechanism of TAGLN2 stabilization and, further, protection of F-actin from cofilin attack is currently undetermined. We can rule out a role in capping of barbed ends, as the proteins in this category significantly affect spontaneous polymerization. Instead, we hypothesize that TAGLN2 binds along the side of actin filaments and may stabilize filaments by altering their structure, as previously reported (Stokes and DeRosier, 1987). Thus, we suggest a "molecular staple" model for TAGLN2-mediated F-actin stabilization, as described in Fig. 5 F. This feature may be especially beneficial for blocking cofilin activity, as cofilin severs actin filaments by increasing their bending and twisting elasticity (McCullough et al., 2011).

Cofilin is a small, ubiquitously expressed protein that is essential for cell survival and for T cell activation. Although cofilin is an actin-severing protein, its activity can favor F-actin polymerization, because cofilin activity generates actin monomers and new barbed ends where active Arp2/3 complexes can associate and promote F-actin elongation (Huang and Burkhardt, 2007). In this regard, it is very interesting to find that cofilin mainly localizes at upper region of d-SMAC—TAGLN2 is rather excluded at this region and enriched at the bottom region—during IS formation. As these two molecules function oppositely in vivo as well as in vitro, these results suggest that TAGLN2 and cofilin may not compete with each other in vivo but rather cooperate to regulate a stable centripetal retrograde actin flow during IS formation. From this point of view, it is interesting that TAGLN2 deficiency results in attenuated cofilin activity in T cells. There are at least two explanations for the down-regulation of cofilin activity in *TAGLN2*$^{-/-}$ T cells. First, *TAGLN2*$^{-/-}$ T cells may attenuate cofilin activity to restore the F-actin content, which was reduced by loss of TAGLN2. Therefore, active cofilin may further exacerbate the deficiency of TAGLN2 in T cells. Alternatively, *TAGLN2*$^{-/-}$ may attenuate actin-linked signaling pathways including PLC, PI3K, and ERK, presumably caused by the immature actin structure at the IS. Indeed, both PI3K and ERK overlap with the Ras-signaling cascade that regulates dephosphorylation of cofilin in human untransformed T cells (Wabnitz et al., 2006). Thus, down-regulation of cofilin activity might be a natural result of attenuated actin-linked signaling in *TAGLN2*$^{-/-}$ T cells.

Another question is why cells do not simply make less cofilin, instead of expressing TAGLN2 to keep actin stable. In this regard, if cellular concentrations of TALN2 are substoichiometric to active cofilin, its role as a cofilin antagonist is unclear. However, we found that the cellular concentration of TAGLN2 is much higher than cofilin in T cells, as determined by quantitative Western blotting (Fig. S5). Moreover, our preliminary results demonstrated that substitution of putative phosphorylation sites in TAGLN2 influences its actin-stabilizing function, while having little effect on F-actin binding (unpublished data). Although more careful experiments are needed to understand how TAGLN2 phosphorylation controls F-actin stabilization, these results strongly suggest that T cells require TAGLN2 to stabilize F-actin levels, thereby controlling T cell function under diverse physiological conditions.

Although intracellular signals such as Zap70 and Erk1/2 are necessary to activate LFA-1, the actin cytoskeleton also plays a role in LFA-1–mediated adhesion (Lub et al., 1997; Sampath et al., 1998). In the present study, increase in T cell conjugation with APC or adhesion to ICAM-1, with WT transfection but not with ΔABM, suggests that actin regulation by TAGLN2 is linked to LFA-1 affinity or avidity changes. However, this fact raises an important question about whether the biological effectiveness of TAGLN2 is primarily caused by actin regulation, a secondary effect stemming from LFA-1 adhesion, or both. The current results show that primary actin signaling is critical, but a secondary function to enhance LFA-1–mediated T cell adhesiveness may also be important, particularly in cases

measured using ELISA. (A and B) All data represent the means ± SD of three independent experiments. *, P < 0.05 versus WT. (C) After 72 h, cell division was monitored by flow cytometry of CFSE-labeled T cells. Data are one representative of three individual experiments, each with three mice per group. (D) After 4-h coincubation of *OTI TCR*$^+$ CD8$^+$ T cells with OVA-loaded or -unloaded EL4 cells, ex vivo cytotoxicity was tested at various ratios of effector/target cells. The data represent the mean ± SD of three independent experiments. *, P < 0.05 versus WT. (E) *OTI TCR*$^+$ CD8$^+$ T cells were stimulated with 200 nM PMA and 1 µM ionomycin, and cellular expression of granzyme B and perforin was determined by flow cytometry. The boxed areas indicate the CD8$^+$ granzyme B^{high} or CD8$^+$ perforin^{high} population. Data are one representative of three individual experiments, each with three mice per group. MFI, mean fluorescence intensity. (F) Under the condition as described in D, secretion levels of granzyme B were measured using ELISA. (G) Conjugate formation was also quantitated after 30-min incubation of *OTI TCR*$^+$ CD8$^+$ T cells with OVA-loaded EL4 cells. (H) *TAGLN2*$^{+/+}$ or *TAGLN2*$^{-/-}$ CD3$^+$ T cells were retrovirally transduced with empty vector (EV), WT-TG2, or TG2ΔABM. Reconstitution was confirmed by Western blotting. Cells were loaded on anti-CD3/28 coverslips for 5 min and stained for TG2 and F-actin. Cell spreading was determined. Images are representative of >50 cells examined. Bar, 5 µm. (I) Cells were also incubated with SEB-pulsed CD19$^+$ B cells for 24 h, and IL-2 levels were measured using ELISA. NT, not treated. (F–I) Data are means ± SD of triplicate experiments. *, P < 0.05 versus empty vector–expressing T cells. $^+$, P < 0.05 versus WT-expressing T cells. (J) Cells were loaded on anti-CD3/28 coverslips, with or without ICAM-1(±ICAM-1). After 10 min, the cells were lysed, and Western blotting was performed, as shown in Fig. 8 (D and E). The data are representative of two independent experiments. KO, knockout; M, molecular mass.

of cytotoxic T lymphocyte–mediated cytotoxicity against target cells. However, further studies are necessary to elucidate how TAGLN2/actin signaling is connected to LFA-1 activation.

In summary, our results indicate that TAGLN2 is a d-SMAC molecule in the IS and plays a key role in mature synapse formation by binding and stabilizing actin. We also provide initial evidence linking TAGLN2 with T cell immunity through its role in cytokine production and cytotoxic effector function. TAGLN2 is the only transgelin family member expressed in immune cells. Moreover, the ability of TAGLN2 to influence activation of T cell immunity may be involved in a variety of immune responses and diseases including cancer, infectious diseases, septic shock, autoimmune diseases, and immediate and delayed type hypersensitivity reactions.

Materials and methods

Reagents and antibodies

Rabbit polyclonal anti-TAGLN2 and anti-GFP antibodies were raised in rabbits using purified full-length TAGLN2 and GFP proteins (AbFrontier). Rabbit polyclonal anti-TAGLN antibody, mouse polyclonal anti-GFP, and anti–PLC-γ antibodies, and goat polyclonal anti–β-actin antibody were purchased from Santa Cruz Biotechnology, Inc. Rabbit polyclonal antibodies against p-PI3K, p-Zap70, Zap70, Lck, ERK, p-ERK, p-PLC-γ, p-PKC-θ, PKC-θ, and p-cofilin; horseradish peroxidase–conjugated anti–mouse IgG; and anti–rabbit IgG antibodies were obtained from Cell Signaling Technology. Mouse monoclonal antibodies against TAGLN3, myosin IIA, Arp3, and cofilin were purchased from Abcam. Anti–human and –mouse CD28 antibodies were acquired from R&D Systems. FITC-conjugated anti–mouse CD4, and peridinin chlorophyll protein complex (PerCP) Cy5.5-conjugated CD8-α antibodies were purchased from eBioscience. Anti–goat IgG, anti–hamster IgG, TRITC-conjugated anti–mouse IgG, TRITC-phalloidin, poly-L-lysine (PLL), and OVA were purchased from Sigma-Aldrich. OKT3 (human anti-CD3; CRL-8001) and 145-2C11 (mouse anti-CD3; CRL-1975) hybridoma cell lines were purchased from the ATCC. TS1/18 (anti–human LFA-1; HB-203) and R6.5 (anti–human ICAM1) hybridoma cell lines were a gift from T.A. Springer (Harvard Medical School, Boston, MA). Lipofectamine 2000 reagent, Alexa Fluor 647 phalloidin, and carboxyfluorescein succinimidyl ester (CFSE) were obtained from Life Technologies. siRNA-targeting *TAGLN2* (M-011468-02; 5′-GCAAGAACGUGAUCGGGUU-3′; 5′-UAUGUGAGCUCAUUAAUGC-3′; 5′-CAACUGGUUCCCUAAGAAA-3′; 5′-UGCAAGCAGCUGAGCGCUA-3′) and a scrambled siRNA (D-001810-01; 5′-UAAGGCUAUGAAGAGAUAC-3′) were obtained as a pool of four siRNA duplexes from Thermo Fisher Scientific. SEE and SEB were obtained from Toxin Technology. OVA 257–264 and OVA 323–339 peptides were purchased from InvivoGen.

Cells

Jurkat T cells (TIB-152; ATCC), A7r5 (CRL-1444; ATCC), HEK293T (CRL-1573; ATCC), CHO-K1 (10061; Korean Cell Line Bank) cells, EL4 (TIB-39; ATCC), and Raji B cells were maintained in RPMI 1640 medium or DMEM medium (Gibco/Invitrogen) supplemented with 10% (vol/vol) FBS (Gibco/Invitrogen). After written informed consent, human primary PBLs were isolated from healthy donors using dextran sedimentation and centrifugation through a discontinuous Ficoll gradient (GE Healthcare). Mouse $CD3^+$ T cells were purified from the mouse spleen and lymph nodes on a T cell enrichment column (R&D Systems). Mouse splenocytes were dispersed and purified to $CD4^+$, $CD8^+$, and $CD19^+$ populations by MACS cell separation (Miltenyi Biotec). The purity of each population was confirmed to be >95% by flow cytometry.

Mice

For generation of TAGLN2 knockout mice, murine genomic DNA for *TAGLN2* was obtained from 129/SvJ mouse J1 embryonic stem (ES) cells by PCR. A targeting vector was constructed to delete nucleotides 14,691–15,479 containing exon 2 of *TAGLN2* using a long arm fragment and two short arm fragments ligated into the pOSDupDel.Neo vector. The targeting vector was then electroporated into 129/SvJ ES cells after linearization using NotI. Positive recombinant ES cells were identified using PCR and then microinjected into C57BL/6 blastocysts. The resulting chimeric mice were then mated with C57BL/6 mice. Germline transmission was confirmed using Southern blot analysis (Macrogen). Interbreeding of the heterozygous mice was performed to generate homozygous TAGLN2-deficient mice.

Transgenic mice expressing GFP or TG2_GFP on T cells were established. The cDNA fragments corresponding to *GFP* or human *TAGLN2_GFP* were subcloned into a transgenic expression vector containing the proximal murine *p56Lck* promoter and the introns and exons of the human growth hormone gene (Chaffin et al., 1990). The resulting plasmids were used to generate transgenic mouse lines according to standard protocols (Macrogen).

Ova-specific TCR transgenic line I (OTI) mice contain transgenic inserts for mouse *Tcra-V2* and *Tcrb-V5* genes for recognition of OVA 257–264 in the context of H2-K^b, and ova-specific TCR transgenic line II (OTII) mice contain transgenic inserts for mouse α-chain and β-chain TCR subunits expressed by a $CD4^+$ T cell hybridoma designated clone 1.1, which is specific for OVA 323–339 in the context of H2-Ab1 (I-A^b; The Jackson Laboratory). *TAGLN2*$^{-/-}$, GFP, and TG2_GFP mice were then crossed with OTI mice to generate *OTI TCR*$^+$*/TAGLN2*$^{-/-}$, *OTI TCR*$^+$/GFP, and *OTI TCR*$^+$/TG2_GFP mice for five generations. *OTII TCR*$^+$*/TAGLN2*$^{-/-}$, *OTII TCR*$^+$/GFP, and *OTII TCR*$^+$/TG2_GFP mice were also generated by backcrossing in the same way as OTI mice. All mouse lines were confirmed by PCR using genomic DNA. All mice were housed in specific pathogen-free conditions, and all experiments were approved by the Animal Care and Use Committee of the School of Life Sciences, Gwangju Institute of Science and Technology.

cDNA constructs

To generate *TAGLN2* constructs, a human *TAGLN2* clone coding for the full-length open reading frame was purchased from ImaGene. The human WT *TAGLN2* coding sequence region was ligated to pCDNA3 vector (cytomegalovirus [CMV] promoter; Invitrogen), pEGFP-N1 vector (CMV promoter; Takara Bio Inc.), and pHJ-1 as a lentiviral vector (CMV promoter). *TAGLN2ΔABM* (Δ154–161) was generated by overlapping PCR. The 408– and 81–base pair products from first-round PCR were used together as an overlapping template to generate *TAGLN2ΔABM*.

To produce His-tagged TAGLN2 and TAGLN2ΔABM recombinant proteins, the pET-28a vector was used as an expression vector, which has a T7 promoter and provides six His residues at the N terminus of the expressed protein. The coding sequences of *TAGLN2* and mutant *TAGLN2* were amplified by PCR, and the products were incorporated into pET-28a. For retroviral transduction to mouse primary T cells, *TAGLN2* and *TAGLN2ΔABM* genes were subcloned into the pRV-GFP vector, which is a retroviral plasmid that directs the expression of GFP.

Cofilin cDNA was amplified from *cofilin* mRNA, and then, the constitutively active mutant *cofilin* (cofilin/S3A) was constructed by substituting Ser-3 with alanine. The PCR product was inserted into pERFP_N1 (CMV promoter; Takara Bio Inc.).

Cell transfection and lentiviral infection

Transient transfection to human PBLs and Jurkat T cells was mostly performed by Amaxa technology using the human T cell nucleofector and nucleofector kitV (Lonza). Transfection to CHO-K1 cells was performed using Lipofectamine 2000 (Life Technologies). To establish stable cell lines, cDNAs in pHJ-1 vector were cotransfected with lentiviral packaging vectors into 293T cells. After 48 h, the supernatants were collected and spin infected into Jurkat T cells by centrifugation at 800 *g* for 30 min in the presence of 8 µg/ml polybrene.

T cell stimulation

Mouse $CD3^+$ T cells, PBLs, and Jurkat T cells were stimulated with 10 µg/ml anti-CD3 (OKT3 for human; 145-2C11 for mouse)/2 µg/ml CD28 and secondary goat or hamster IgG antibody (5 µg/ml) for the times indicated in the text. In some cases, T cells were stimulated by 25 µg/ml anti-CD3/2 µg/ml CD28 with or without ICAM-1–coated coverslips. For superantigen stimulation, T cells were incubated with 1 µg/ml SEE-pulsed Raji B cells or 1 µg/ml SEB-pulsed mouse $CD19^+$ B cells. For OVA stimulation, $CD4^+$ and $CD8^+$ T cells isolated from spleens of *OTII TCR*$^+$*/TAGLN2*$^{+/+,-/-}$ and *OTI TCR*$^+$*/TAGLN2*$^{+/+,-/-}$ mice, respectively, were cultured with T cell–depleted splenocytes pulsed with 10 µg/ml of OVA 323–339 (OTII) and OVA 257–264 (OTI) for 24 h.

Western blot and Northern blot analysis

Cells or homogenized tissues from a C57BL/6 mouse were lysed in ice-cold lysis buffer (50 mM Tris-HCl, pH 7.4, containing 150 mM NaCl, 1% Triton X-100, one tablet of Complete protease inhibitors, and phosphatase inhibitors) for 1 h on ice. Cell lysates were centrifuged at 16,000 *g* for

25 min at 4°C, and the supernatant was eluted with SDS sample buffer (100 mM Tris-HCl, pH 6.8, 4% SDS, and 20% glycerol with bromophenol blue) and heated for 5 min. The proteins were separated through 10–12% SDS-PAGE gels and were transferred to a nitrocellulose membrane by means of Trans-Blot SD semidry transfer cell (Bio-Rad Laboratories). The membrane was blocked in 5% skim milk (1 h), rinsed, and incubated with intended antibodies in TBS containing 0.1% Tween 20 (TBS-T) and 3% skim milk overnight. Excess primary antibody was then removed by washing the membrane four times in TBS-T. The membrane was then incubated with 0.1 µg/ml peroxidase-labeled secondary antibody (anti–rabbit or –mouse) for 1.5 h. After three washes with TBS-T, bands were visualized by Western Blotting Detection reagents (iNtRON Biotechnology) and were then exposed to x-ray film.

For Northern blot analysis, human Northern RNA blot (12 major tissues; OriGene) was hybridized with *TAGLN2* (5′-GCTGAGCGCTATGGCATTAACACCACTGAC-3′) and *β-actin* (5′-GGGAAATCGTGCGTGACATTAAGGAGAAGC-3′) cDNAs as probes labeled with α-[^{32}P]dCTP (PerkinElmer) by random priming using the Prime-It kit (Agilent Technologies), according to the manufacturer's protocol. Blots were prehybridized for 30–60 min at 68°C in Rapid-hyb buffer (GE Healthcare) and hybridized for 90 min at 68°C in the presence of cDNA probes, following the protocol provided. Blots were washed three times in 2× SSC/0.05% SDS at room temperature for 10 min and twice in 0.1× SSC/0.1% SDS at 68°C for 5 min then exposed to x-ray film with intensifying screens at −70°C.

RT-PCR and real-time qPCR

Total RNA was isolated from cells or homogenized tissues of C57BL/6 mice with TRI Reagent (Molecular Research Center, Inc.) and reverse transcribed using RT Premix (iNtRON Biotechnology). PCR was performed with the following primers (the respective forward and reverse pairs are indicated): human *IL2*, 5′-CACGTCTTGCACTTGTCAC-3′ and 5′-CCTTCTTGGGCATGTAAAACT-3′; mouse *IL2*, 5′-TGAGCAGGATGGAGAATTACAGG-3′ and 5′-GTCCAAGTTCATCTTCTAGGCAC-3′; human *GAPDH*, 5′-CGGAGTCAACGGATTTGGTCGTAT-3′ and 5′-AGCCTTCTCCATGGTGGTGAAGAC-3′; mouse *GAPDH*, 5′-GCACAGTCAAGGCCGAGAAT-3′ and 5′-GCCTTCTCCATGGTGGTGAA-3′; and mouse *TAGLN2*, 5′-GGTGCAGCAGAAGATTGAGAA-3′ and 5′-GATCTTCTTTACTGGGGCCTG-3′. The amplification protocol consisted of denaturation at 94°C for 30 s, annealing at 60–62°C for 20 s, and extension at 72°C for 40 s. The 30 cycles were preceded by denaturation at 72°C for 7 min. The expression levels of the human and mouse *IL2* genes were evaluated by real-time RT-PCR, unless otherwise indicated. PCR amplification was performed in StepOne Real-Time PCR Systems (Applied Biosystems) for continuous fluorescence detection in a total volume of 10 µl of cDNA/control and gene-specific primers by using SYBR Premix *Ex Taq* (Takara Bio Inc.). The mRNA levels of the target genes, relative to *GAPDH*, were normalized using the following formula: relative mRNA expression = $2^{-(\Delta Ct \text{ of target gene} - \Delta Ct \text{ of GAPDH})}$, where Ct is the threshold cycle value. In each sample, the expression of the analyzed gene was normalized to that of *GAPDH* and described as the mRNA level relative to *GAPDH*.

Live imaging

For dynamic T cell imaging, J-GFP and J-TG2_GFP cells were transiently transfected with LifeAct (mCherry) by using Amaxa (Lonza) and plated on coverslips (18-nm diameter; Marienfeld) coated with human anti-CD3/28. After preincubation, time-lapse series of randomly selected, LifeAct-positive cells in imaging medium (137 mM NaCl, 5 mM KCl, 1 mM sodium phosphate, 6 mM D-glucose, 1 mM $CaCl_2$, 0.5 mM $MgCl_2$, 1% BSA, and 10 mM Hepes, pH 7.3) at 37°C were imaged using a 100×, NA 1.40 oil immersion objective of a laser-scanning confocal microscope (FV1000; Olympus). Images from the bottom area of each coverslip were recorded every 20 s for a total of 1,000 s. For F-actin accumulation at T cell–B cell contact sites, SEE-loaded Raji B cells (stained for ICAM-1 with cy5-conjugated CBRIC1/11) were mixed with T cells and preincubated in solution for 10 min. After incubation, conjugated cells were placed on PLL-coated coverslips and initiated imaging. Time-lapse and z-stack images were collected every 10 min, for a total of 120 min at 37°C. The data were obtained, processed, and analyzed by FLUOVIEW software (Olympus).

Immunofluorescence and confocal microscopy

For immunofluorescence staining, T cells were incubated for 5 min or indicated times on PLL or human or mouse anti-CD3/28–coated coverslips. CHO-K1 cells were incubated for 2 h on 10 µg/ml fibronectin-coated coverslips. The cells were fixed, washed with PBS, and permeabilized with 0.1% Triton X-100 in PBS for 10 min. The cells were then blocked with 1% BSA in PBS for 1 h, rinsed with PBS, and incubated with primary antibodies in blocking buffer overnight at 4°C. Secondary antibodies were added after washing, incubated for 1 h at room temperature in the dark, rinsed with PBS, and incubated for 30 min at room temperature with TRITC-phalloidin or Alexa Fluor 647–phalloidin in PBS to stain actin. The cells were then washed and mounted with Fluorescent Mounting Medium (Dako). Images were obtained using a 100×, NA 1.40 oil immersion objective of a laser-scanning confocal microscope (FV1000). For the 3D localization assay, z stacks were generated from optical sections taken at 0.2-µm intervals, and FLUOVIEW program and Volocity software (PerkinElmer) were used for 3D image reconstruction.

Image analysis

The fluorescence intensity profiles were measured by the FLUOVIEW program. To determine the percentage of F-actin ring formation on anti-CD3/28–coated coverslips, actin rings were assessed as ring (R), partial (P), and not cleared (N) and quantified using the following equation: percentage of actin ring formation = (R + P)/(R + P + N) × 100. Actin accumulation at the contact sites in the T cells during IS formation was calculated as the ratio between the mean fluorescence intensity of LifeAct in the half portion of contact side (a) and distal side (b) in the T cells. At least 50–100 cells or conjugates were counted in each of three independent experiments. All data were plotted using KaleidaGraph (Synergy Software).

Cell adhesion assay

96-well flat-bottom plates (Thermo Fisher Scientific) were coated with human or mouse rICAM-1-Fc (R&D Systems) or 1% BSA (Sigma-Aldrich) as a negative control. Cells were labeled with 0.5 µM BCECF (2′,7′-bis-(2-carboxyethyl)-5-(and-6)-carboxyfluorescein; Invitrogen), washed, resuspended in culture media, and then pretreated with or without 10 µg/ml TS1/18 or 2 µM Cyt D. For TCR stimulation, cells were incubated for 30 min at 37°C in media supplemented with anti-CD3/CD28 antibodies. T cells were added in triplicate to coated plates (10^5 cells/well) containing secondary anti-IgG as a cross-linker and incubated for 30 min at 37°C. Input was determined by using a fluorescence plate reader (Molecular Devices). Unbound cells were removed by washing three times with warm PBS, and cell adhesion was calculated by dividing the fluorescence emission of bound cells by the total emission of all cells seeded per well.

Conjugation assay

Jurkat T cells and Raji B cells were stained with CellTracker Orange CMTMR (5-(and-6)-((4-chloromethyl)benzoyl) amino) and Green CMFDA (5-chloromethylfluorescein diacetate), respectively, according to the manufacturer's protocol (Invitrogen). Raji B cells (2×10^5) were incubated with 5 µg/ml SEE or vehicle control for 30 min, washed, and resuspended in RPMI 1640 medium. For a blocking experiment, Jurkat T cells were incubated with TS1/18, TS2/4 (10 µg/ml each), and Cyt D (2 µM) for 30 min. For conjugation, equal volumes of B and T cells were mixed and incubated at 37°C for indicated time points. The relative proportion of orange, green, and orange–green events in each tube was determined by two-color flow cytometry using a FACSCanto instrument (BD) and analyzed with FlowJo software (Tree Star). The number of gated events counted per sample was at least 20,000. The percentage of conjugated T cells was determined as the number of dual-labeled (CMFDA and CMTMR positive) events divided by the number of CMFDA-positive T cells. Mouse $CD3^+$ T cells and SEB-loaded $CD19^+$ B cells conjugates were also stained, incubated, and determined as described as described in Jurkat T cell–Raji B cell conjugation assay.

In cytotoxic T cell–target cell conjugation assay, $CD8^+$ T cells from *OTI TCR$^+$/TAGLN2$^{+/+}$* or *OTI TCR$^+$/TAGLN2$^{-/-}$* mice were stimulated in vitro by OVA 257–264 peptide-loaded DCs in the presence of 10 U/ml rIL-2 to generate OVA-specific cytotoxic T cells. 2 d after stimulation, cells were washed and seeded into new media daily for 3–6 d. OVA-specific cytotoxic T cells were purified by MACS beads, and mixed with EL4 cells, which were used as target cells, loaded with 10 µg/ml OVA 257–264 peptide for 1 h. Conjugates were determined as described in the previous paragraph.

Purification of recombinant proteins

Expression of recombinant proteins in *Escherichia coli* BL21 (DE3) cells followed the protocol used for transformation of the aforementioned recombinant plasmids. Expression of recombinant proteins was induced by addition of 0.3 mM IPTG to culture media for 4 h at 37°C, and then, cells were collected.

The cell pellets were resuspended in PBS, sonicated, and centrifuged. After centrifugation, recombinant proteins in the supernatant were purified by affinity chromatography on a His-selected Nickel Affinity Gel (Sigma-Aldrich). The gel was equilibrated with 10 volumes of buffer (50 mM sodium phosphate, pH 8.0, and 0.3 M NaCl) and incubated with the supernatant. The gel was washed with 5 volumes of wash buffer (50 mM sodium phosphate, pH 8.0, 0.3 M NaCl, and 10 mM imidazole). The protein was eluted with increasing concentrations of imidazole up to 250 mM, and the collected fractions were dialyzed to remove imidazole. The proteins were assessed by SDS-PAGE and Coomassie blue staining.

In vitro actin cosedimentation assays

Actin cosedimentation assays were performed as described previously (Kwon et al., 2013). Nonmuscle actin derived from human platelets was purchased (Cytoskeleton, Inc.). Unless otherwise indicated, actin was used at a final concentration of 4 µM. Actin was mixed in G buffer (0.2 mM $CaCl_2$, 0.2 mM ATP, and 5 mM Tris-HCl, pH 8.0) to produce an actin stock. Actin was polymerized in APB (50 mM KCl, 2 mM $MgCl_2$, 0.2 mM ATP, and 5 mM Tris-HCl, pH 8.0) at room temperature for 1 h and then incubated with His-tagged TAGLN2 (8–24 µM) for 30 min at room temperature. 1 µM α-actinin and 1 µM BSA were used as positive and negative controls. Actin filaments with bound proteins were pelleted by centrifugation at 100,000 *g* for 2 h (for the F-actin binding assay) or 10,000 *g* for 10 min (for the F-actin bundling assay) at room temperature. Equal amounts of pellet and supernatant were resolved using SDS-PAGE, and proteins were visualized by Coomassie blue staining. The percentage of actin in supernatant and pellet was quantified densitometrically using ImageJ (National Institutes of Health).

Quantification of binding data

Quantitation of actin binding affinity was performed as previously described (Kwon et al., 2013). In brief, the intensity ratio of recombinant protein to F-actin in each pellet was converted to a molar ratio (TAGLN2/actin) using standard curves run on each gel that contained known amounts of TAGLN2 (0.4–5.6 µM) and actin (4 µM) in molar/molar ratios. Cosedimentation binding data were plotted as a function of the free TAGLN2 concentration added and fitted according to the equation: $[C_{bound}]/[actin] = B_{max}[C_{free}]/K_d + [C_{free}]$, where $[C_{bound}]$ and $[C_{free}]$ are the bound and free concentrations of TAGLN2, [actin] is the total actin concentration, B_{max} is the maximal molar binding ratio, and K_d is the dissociation constant (micromolars). Data were fit using the Excel Solver package (Microsoft) by varying the values of B_{max} and K_d and minimizing the sum of squares between the actual and predicted binding ratios.

Actin polymerization assay

Actin polymerization assays were performed using the Actin Polymerization Biochem kit (Cytoskeleton, Inc.) in which the rate of conversion of pyrene-labeled G-actin into F-actin was monitored. In brief, pyrene-labeled G-actin was thawed at 4°C and centrifuged at 14,000 *g* for 30 min at 4°C to remove residual F-actin. Unless otherwise indicated, 4 µM G-actin, 10 nM bovine brain Arp2/3 complex (Cytoskeleton, Inc.), recombinant human GST-tagged VCA domain of WASp (400 nM; Cytoskeleton, Inc.), and His-tagged TAGLN2 (4 µM) were used for polymerization assay. Actin polymerization was initiated by adding G-actin stock to the wells with APB and target proteins. The plate was read with a fluorometer (GEMINI XS; Molecular Probe), with excitation at 355 nm and emission at 405 nm. Fluorescence data were zeroed by subtracting baseline fluorescence from all fluorescence values and normalized by dividing all fluorescence values by the mean fluorescence of at the plateau.

Actin depolymerization assay

For monitoring actin filament disassembly, 20 µM pyrene G-actin was polymerized in APB for 1 h in the presence or absence of various concentrations of TAGLN2 or phalloidin (20 µM; Cytoskeleton, Inc.). Reactants were then diluted to 4 µM with G-actin buffer to induce spontaneous depolymerization. In the case of cofilin-mediated depolymerization, 1 µM cofilin (Cytoskeleton, Inc.) in G-buffer was added to F-actin reactants during the dilution step. Decreasing pyrene fluorescence was measured as in the actin polymerization assay. Normalization for fluorescence intensity was performed by dividing fluorescence value of reactants with fluorescence value of the reactant in the presence of phalloidin at each time point. Changes in fluorescence intensity (ΔF) during depolymerization were calculated by subtracting the fluorescence measured at last time point from the fluorescence measured at initial time point. Changes of each sample (ΔF of TAGLN2 or TAGLN2 + cofilin) were subsequently divided by ΔF of cofilin.

Visualization of actin filaments by confocal microscopy

4 µM G-actin was incubated with APB in the presence or absence of 8 µM TAGLN2 conjugated with Dylight488 (Thermo Fisher Scientific) for 30 min at room temperature. One-tenth of the reaction volume was subsequently stained with TRITC-phalloidin and placed on a PLL-coated coverslip. In some cases, G-actin was exchanged with 4 µM 488-actin (Hypermol), and mixed with TAGLN2 (0–8 µM) and cofilin (0–1 µM) on coverslips coated by *N*-ethylmaleimide–myosin II. The fluorescent images were collected using confocal microscopy.

EM analysis

Negative staining was used to visualize F-actin under EM. After actin polymerization, the samples were loaded onto cooper grids coated with Formvar and carbon for 30 s and excess liquid was removed with filter paper. Actin bound on the grids was stained with 1% uranyl acetate (Sigma-Aldrich) for 10 min and then washed with distilled water. Excess liquid was removed, and grids were air dried. EM observation was performed using a transmission electron microscope (TECNAI G2; FEI) operated at 120 kV.

Determination of cellular F-actin content

Jurkat T cells or mouse T cells were maintained in serum-free medium for 12 h and incubated with anti-CD3/28 for the indicated times at 37°C. The reactions were terminated by adding 4% paraformaldehyde. Fixed cells were washed once with PBS and resuspended in PBS containing 1% BSA and 0.25% Triton X-100 for 5 min. After permeabilization, cells were washed, stained for 30 min with TRITC-phalloidin, and then analyzed by flow cytometry.

Structural modeling of TAGLN2

The crystal structure of human TAGLN1 was used as a template to superimpose a TAGLN2 monomer on each of two TAGLN1 molecules using the online server SuperPose (Maiti et al., 2004). In addition, the prediction of a TAGLN2 homodimer was performed computationally by the ClusPro online server, and the same interface was observed as for the TAGLN1 template. Interactions of the TAGLN2 homodimer were analyzed by University of California, San Francisco Chimera and Discovery Studio Visualizer software (Accelrys Software, Inc.) and optimized by virtual inspection to overcome the steric hindrances.

Detection of cell surface proteins and intracellular granzyme B and perforin

Jurkat T cells, mouse splenocytes, T cells, B cells, and DCs were suspended in PBS containing 2% FBS. Cells were stained with fluorescence-conjugated antibodies against human CD3-ε, CD28, LFA-1, ICAM-1, and mouse CD4, CD8, CD3-ε, CD28, B220, CD11c, MHCII, CD86, and CD80 for 30 min at 4°C. The corresponding isotype controls were used in each antibodies. For intracellular granzyme B and perforin staining, OVA-specific cytotoxic T cells were restimulated with 200 nM PMA and 1 µM ionomycin for 4 h at 37°C. Brefeldin A was added during the last 2 h of restimulation. Cells were stained with anti-CD8, and then fixed, permeabilized, and stained with antibodies specific for granzyme B and perforin (eBioscience). Cells were acquired on a FACSCanto, and data were analyzed with FlowJo software.

Measurement of secretion of cytokines and granzyme B

Splenic $CD3^+$, $CD4^+$, or $CD8^+$ T cells (5×10^4 cells/sample) were stimulated as described in T cell activation section. After 24–48 h, the amounts of IL-2 and IFN-γ in the supernatants were determined by ELISA with Duo Set Mouse ELISA kits (R&D Systems). To measure granzyme B secretion, OVA-specific cytotoxic T cells generated previously described in Conjugation assay section were restimulated with EL4 cells loaded with 10 µg/ml OVA 257–264 at a 20:1 (effector cells/target cells) ratio for 4 h. The amounts of granzyme B in the supernatants were determined by ELISA.

T cell proliferation assay

$CD4^+$ and $CD8^+$ T cells were labeled for 30 min at 37°C with 10 µM CFSE (Molecular Probe) and washed twice in PBS. Labeled T cells were stimulated with anti-CD3/28 antibodies. After 72 h, T cells were collected and analyzed by flow cytometry for dilution of CFSE intensity.

In vitro cytotoxic assay

For the in vitro cytotoxic T cell activity assay, OVA-specific T cells were generated and incubated with target cells described in Measurement of secretion of cytokines and granzyme B section at various ratios of effector cells to target cells. After 4 h, cell-mediated cytotoxicity was determined using CytoTox 96 NonRadioactive cytotoxicity assay kit (Promega), and the percentage of cytotoxicity was calculated according to manufacturer's instructions.

Retroviral transduction in mouse T cells

Before retroviral transduction, mouse $CD3^+$ T cells from *TAGLN2*$^{+/+}$ and *TAGLN2*$^{-/-}$ mice were incubated in 10 µg/ml anti-CD3–coated coverslips with 2 µg/ml anti-CD28 and 10 µg/ml rIL-2 for 48 h. A total of 6×10^6 retroviral packaging cells (platinum-E cells; Cell Biolabs) were plated overnight in 10-cm^2 dishes. Retroviral particles were generated by transfection with retroviral vectors (empty vector, TG2, and TG2ΔABM) and pCL-Eco packaging vector using Lipofectamine 2000 (Invitrogen). After 48 h, virus supernatants (1 ml) were harvested, mixed with 10^6 mouse T cells and polybrene (8 µg/ml) in a 12-well plate and centrifuged for 90 min at 2,000 *g* at 32°C with 20 U/ml rIL-2. The transduced T cells were maintained with fresh media with rIL-2 and expanded for 5–8 d.

Statistics

Mean values were calculated using data taken from at least three independent experiments conducted on different days. Where significance testing was performed, unpaired Student's *t* tests and one-way analysis of variance tests were used. Differences between groups were considered significant at $P < 0.05$.

Online supplemental material

Fig. S1 shows that TAGLN2 is expressed in immunogenic tissues and cells and knockdown of TAGLN2 reduces T cell activation. Fig. S2, which corresponds to Fig. 1 F, shows individual z-stack images acquired as optical sections from bottom to top. Fig. S3 shows the strategy to generate TAGLN2 knockout mice and characterization of their population, development, and expression of indicated surface molecules. Fig. S4 shows the strategy to generate GFP-T or TG2_GFP-T transgenic mice and characterization of their T cell development and cytokine secretion in response to TCR activation. Fig. S5 shows the cellular concentrations of TAGLN2, cofilin, and actin, as determined by quantitative Western blotting. Video 1, corresponding to Fig. 1 E, shows a 3D view of TAGLN2_GFP and ICAM-1 localization at the contact site of Jurkat T cells and Raji B cells. Videos 2–4, corresponding to Fig. 1 F, show localization of TAGLN2, Arp3, myosin IIA, and F-actin in Jurkat T cells placed on anti-CD3/28–coated coverslips. Videos 5 and 6, corresponding to Fig. 2 A, show real-time F-actin ring formation and dynamic localization of TAGLN2 and actin during J-GFP or J-TG2_GFP cell spreading on anti-CD3/28–coated coverslips. Videos 7 and 8, corresponding to Fig. 8 B, show colocalization of cofilin, TAGLN2, and F-actin in Jurkat T cells placed on anti-CD3/28–coated coverslips. Online supplemental material is available at http://www.jcb.org/cgi/content/full/jcb.201407130/DC1.

Image acquisition was performed using the imaging facility of the Bio-Imaging Research Center at the Gwangju Institute of Science and Technology (GIST).

This work was supported by the Bio & Medical Technology Development Program (2011-0030157), Basic Science Research Program (2012R1A2A1A03002115), Basic Science Research Program through the National Research Foundation of Korea funded by the Ministry of Education (2013R1A6A3A04064259), and Cell Dynamics Research Center Program (2007-0056244) through the National Research Foundation grants funded by the Ministry of Science, ICT (Imagination, Creativity, and Science Technology) and Future Planning, Korea. This work was also partially supported by the Bio-Imaging Research Center at GIST.

The authors declare no competing financial interests.

Submitted: 28 July 2014
Accepted: 27 February 2015

References

Babich, A., S. Li, R.S. O'Connor, M.C. Milone, B.D. Freedman, and J.K. Burkhardt. 2012. F-actin polymerization and retrograde flow drive sustained PLCγ1 signaling during T cell activation. *J. Cell Biol.* 197:775–787. http://dx.doi.org/10.1083/jcb.201201018

Blanchoin, L., K.J. Amann, H.N. Higgs, J.B. Marchand, D.A. Kaiser, and T.D. Pollard. 2000. Direct observation of dendritic actin filament networks nucleated by Arp2/3 complex and WASP/Scar proteins. *Nature*. 404:1007–1011. http://dx.doi.org/10.1038/35010008

Burn, P., A. Kupfer, and S.J. Singer. 1988. Dynamic membrane-cytoskeletal interactions: specific association of integrin and talin arises in vivo after phorbol ester treatment of peripheral blood lymphocytes. *Proc. Natl. Acad. Sci. USA*. 85:497–501. http://dx.doi.org/10.1073/pnas.85.2.497

Camoretti-Mercado, B., S.M. Forsythe, M.M. LeBeau, R. Espinosa III, J.E. Vieira, A.J. Halayko, S. Willadsen, B. Kurtz, C. Ober, G.A. Evans, et al. 1998. Expression and cytogenetic localization of the human SM22 gene (TAGLN). *Genomics*. 49:452–457. http://dx.doi.org/10.1006/geno.1998.5267

Chaffin, K.E., C.R. Beals, T.M. Wilkie, K.A. Forbush, M.I. Simon, and R.M. Perlmutter. 1990. Dissection of thymocyte signaling pathways by in vivo expression of pertussis toxin ADP-ribosyltransferase. *EMBO J.* 9:3821–3829.

Delon, J., K. Kaibuchi, and R.N. Germain. 2001. Exclusion of CD43 from the immunological synapse is mediated by phosphorylation-regulated relocation of the cytoskeletal adaptor moesin. *Immunity*. 15:691–701. http://dx.doi.org/10.1016/S1074-7613(01)00231-X

Eibert, S.M., K.-H. Lee, R. Pipkorn, U. Sester, G.H. Wabnitz, T. Giese, S.C. Meuer, and Y. Samstag. 2004. Cofilin peptide homologs interfere with immunological synapse formation and T cell activation. *Proc. Natl. Acad. Sci. USA*. 101:1957–1962. http://dx.doi.org/10.1073/pnas.0308282100

Freiberg, B.A., H. Kupfer, W. Maslanik, J. Delli, J. Kappler, D.M. Zaller, and A. Kupfer. 2002. Staging and resetting T cell activation in SMACs. *Nat. Immunol.* 3:911–917. http://dx.doi.org/10.1038/ni836

Glenney, J.R., Jr., P. Kaulfus, P. Matsudaira, and K. Weber. 1981. F-actin binding and bundling properties of fimbrin, a major cytoskeletal protein of microvillus core filaments. *J. Biol. Chem.* 256:9283–9288.

Gomez, T.S., K. Kumar, R.B. Medeiros, Y. Shimizu, P.J. Leibson, and D.D. Billadeau. 2007. Formins regulate the actin-related protein 2/3 complex-independent polarization of the centrosome to the immunological synapse. *Immunity*. 26:177–190. http://dx.doi.org/10.1016/j.immuni.2007.01.008

Gordón-Alonso, M., M. Sala-Valdés, V. Rocha-Perugini, D. Pérez-Hernández, S. López-Martín, A. Ursa, S. Alvarez, T.V. Kolesnikova, J. Vázquez, F. Sánchez-Madrid, and M. Yáñez-Mó. 2012. EWI-2 association with α-actinin regulates T cell immune synapses and HIV viral infection. *J. Immunol.* 189:689–700. http://dx.doi.org/10.4049/jimmunol.1103708

Grakoui, A., S.K. Bromley, C. Sumen, M.M. Davis, A.S. Shaw, P.M. Allen, and M.L. Dustin. 1999. The immunological synapse: a molecular machine controlling T cell activation. *Science*. 285:221–227. http://dx.doi.org/10.1126/science.285.5425.221

Han, M., L.-H. Dong, B. Zheng, J.-H. Shi, J.-K. Wen, and Y. Cheng. 2009. Smooth muscle 22 alpha maintains the differentiated phenotype of vascular smooth muscle cells by inducing filamentous actin bundling. *Life Sci.* 84:394–401. http://dx.doi.org/10.1016/j.lfs.2008.11.017

Higgs, H.N., and T.D. Pollard. 2001. Regulation of actin filament network formation through ARP2/3 complex: activation by a diverse array of proteins. *Annu. Rev. Biochem.* 70:649–676. http://dx.doi.org/10.1146/annurev.biochem.70.1.649

Huang, Y., and J.K. Burkhardt. 2007. T-cell-receptor-dependent actin regulatory mechanisms. *J. Cell Sci.* 120:723–730. http://dx.doi.org/10.1242/jcs.000786

Ichetovkin, I., W. Grant, and J. Condeelis. 2002. Cofilin produces newly polymerized actin filaments that are preferred for dendritic nucleation by the Arp2/3 complex. *Curr. Biol.* 12:79–84. http://dx.doi.org/10.1016/S0960-9822(01)00629-7

Kim, J., M.J. Shapiro, A.O. Bamidele, P. Gurel, P. Thapa, H.N. Higgs, K.E. Hedin, V.S. Shapiro, and D.D. Billadeau. 2014. Coactosin-like 1 antagonizes cofilin to promote lamellipodial protrusion at the immune synapse. *PLoS ONE*. 9:e85090. http://dx.doi.org/10.1371/journal.pone.0085090

Kwon, M.-S., K.R. Park, Y.-D. Kim, B.-R. Na, H.-R. Kim, H.-J. Choi, I. Piragyte, H. Jeon, K.H. Chung, W.K. Song, et al. 2013. Swiprosin-1 is a novel actin bundling protein that regulates cell spreading and migration. *PLoS ONE*. 8:e71626. http://dx.doi.org/10.1371/journal.pone.0071626

Larghi, P., D.J. Williamson, J.-M. Carpier, S. Dogniaux, K. Chemin, A. Bohineust, L. Danglot, K. Gaus, T. Galli, and C. Hivroz. 2013. VAMP7 controls T cell activation by regulating the recruitment and phosphorylation of vesicular Lat at TCR-activation sites. *Nat. Immunol.* 14:723–731. http://dx.doi.org/10.1038/ni.2609

Li, M., S. Li, Z. Lou, X. Liao, X. Zhao, Z. Meng, M. Bartlam, and Z. Rao. 2008. Crystal structure of human transgelin. *J. Struct. Biol.* 162:229–236. http://dx.doi.org/10.1016/j.jsb.2008.01.005

Lub, M., Y. van Kooyk, S.J. van Vliet, and C.G. Figdor. 1997. Dual role of the actin cytoskeleton in regulating cell adhesion mediated by the integrin lymphocyte function-associated molecule-1. *Mol. Biol. Cell*. 8:341–351. http://dx.doi.org/10.1091/mbc.8.2.341

Maiti, R., G.H. Van Domselaar, H. Zhang, and D.S. Wishart. 2004. SuperPose: a simple server for sophisticated structural superposition. *Nucleic Acids Res.* 32(Suppl. 2):W590–W594. http://dx.doi.org/10.1093/nar/gkh477

McCullough, B.R., E.E. Grintsevich, C.K. Chen, H. Kang, A.L. Hutchison, A. Henn, W. Cao, C. Suarez, J.-L. Martiel, L. Blanchoin, et al. 2011. Cofilin-linked changes in actin filament flexibility promote severing. *Biophys. J.* 101:151–159. http://dx.doi.org/10.1016/j.bpj.2011.05.049

Monks, C.R., B.A. Freiberg, H. Kupfer, N. Sciaky, and A. Kupfer. 1998. Three-dimensional segregation of supramolecular activation clusters in T cells. *Nature*. 395:82–86. http://dx.doi.org/10.1038/25764

Mori, K., Y. Muto, J. Kokuzawa, T. Yoshioka, S. Yoshimura, T. Iwama, Y. Okano, and N. Sakai. 2004. Neuronal protein NP25 interacts with F-actin. *Neurosci. Res.* 48:439–446. http://dx.doi.org/10.1016/j.neures.2003.12.012

Moriyama, K., K. Iida, and I. Yahara. 1996. Phosphorylation of Ser-3 of cofilin regulates its essential function on actin. *Genes Cells*. 1:73–86. http://dx.doi.org/10.1046/j.1365-2443.1996.05005.x

Pruyne, D., M. Evangelista, C. Yang, E. Bi, S. Zigmond, A. Bretscher, and C. Boone. 2002. Role of formins in actin assembly: nucleation and barbed-end association. *Science*. 297:612–615. http://dx.doi.org/10.1126/science.1072309

Rho, J.-H., M.H.A. Roehrl, and J.Y. Wang. 2009. Tissue proteomics reveals differential and compartment-specific expression of the homologs transgelin and transgelin-2 in lung adenocarcinoma and its stroma. *J. Proteome Res.* 8:5610–5618. http://dx.doi.org/10.1021/pr900705r

Rothlein, R., and T.A. Springer. 1986. The requirement for lymphocyte function-associated antigen 1 in homotypic leukocyte adhesion stimulated by phorbol ester. *J. Exp. Med.* 163:1132–1149. http://dx.doi.org/10.1084/jem.163.5.1132

Sampath, R., P.J. Gallagher, and F.M. Pavalko. 1998. Cytoskeletal interactions with the leukocyte integrin beta2 cytoplasmic tail. Activation-dependent regulation of associations with talin and alpha-actinin. *J. Biol. Chem.* 273:33588–33594. http://dx.doi.org/10.1074/jbc.273.50.33588

Samstag, Y., S.M. Eibert, M. Klemke, and G.H. Wabnitz. 2003. Actin cytoskeletal dynamics in T lymphocyte activation and migration. *J. Leukoc. Biol.* 73:30–48. http://dx.doi.org/10.1189/jlb.0602272

Shapland, C., J.J. Hsuan, N.F. Totty, and D. Lawson. 1993. Purification and properties of transgelin: a transformation and shape change sensitive actin-gelling protein. *J. Cell Biol.* 121:1065–1073. http://dx.doi.org/10.1083/jcb.121.5.1065

Stokes, D.L., and D.J. DeRosier. 1987. The variable twist of actin and its modulation by actin-binding proteins. *J. Cell Biol.* 104:1005–1017. http://dx.doi.org/10.1083/jcb.104.4.1005

Stokes, D.L., and D.J. DeRosier. 1991. Growth conditions control the size and order of actin bundles in vitro. *Biophys. J.* 59:456–465. http://dx.doi.org/10.1016/S0006-3495(91)82239-1

Tavano, R., R.L. Contento, S.J. Baranda, M. Soligo, L. Tuosto, S. Manes, and A. Viola. 2006. CD28 interaction with filamin-A controls lipid raft accumulation at the T-cell immunological synapse. *Nat. Cell Biol.* 8:1270–1276. http://dx.doi.org/10.1038/ncb1492

van der Flier, A., and A. Sonnenberg. 2001. Structural and functional aspects of filamins. *Biochim. Biophys. Acta*. 1538:99–117. http://dx.doi.org/10.1016/S0167-4889(01)00072-6

Wabnitz, G.H., G. Nebl, M. Klemke, A.J. Schröder, and Y. Samstag. 2006. Phosphatidylinositol 3-kinase functions as a Ras effector in the signaling cascade that regulates dephosphorylation of the actin-remodeling protein cofilin after costimulation of untransformed human T lymphocytes. *J. Immunol.* 176:1668–1674. http://dx.doi.org/10.4049/jimmunol.176.3.1668

Wang, C., S.C. Morley, D. Donermeyer, I. Peng, W.P. Lee, J. Devoss, D.M. Danilenko, Z. Lin, J. Zhang, J. Zhou, et al. 2010. Actin-bundling protein L-plastin regulates T cell activation. *J. Immunol.* 185:7487–7497. http://dx.doi.org/10.4049/jimmunol.1001424

Yi, J., X.S. Wu, T. Crites, and J.A. Hammer III. 2012. Actin retrograde flow and actomyosin II arc contraction drive receptor cluster dynamics at the immunological synapse in Jurkat T cells. *Mol. Biol. Cell*. 23:834–852. http://dx.doi.org/10.1091/mbc.E11-08-0731

Yu, Y., A.A. Smoligovets, and J.T. Groves. 2013. Modulation of T cell signaling by the actin cytoskeleton. *J. Cell Sci.* 126:1049–1058. http://dx.doi.org/10.1242/jcs.098210

Zhang, J.C.L., B.P. Helmke, A. Shum, K. Du, W.W. Yu, M.M. Lu, P.F. Davies, and M.S. Parmacek. 2002. SM22β encodes a lineage-restricted cytoskeletal protein with a unique developmentally regulated pattern of expression. *Mech. Dev.* 115:161–166. http://dx.doi.org/10.1016/S0925-4773(02)00088-6

Zhang, Y., Y. Ye, D. Shen, K. Jiang, H. Zhang, W. Sun, J. Zhang, F. Xu, Z. Cui, and S. Wang. 2010. Identification of transgelin-2 as a biomarker of colorectal cancer by laser capture microdissection and quantitative proteome analysis. *Cancer Sci.* 101:523–529. http://dx.doi.org/10.1111/j.1349-7006.2009.01424.x